Delft University of Technology

The influential parameters affecting the vibration intensities in the vicinity of railway tracks

Mohamed Ellithi

November, 2020

Delft University of Technology

The influential parameters affecting the vibration intensities in the vicinity of railway tracks

by

Mohamed Ellithi

M.Sc. Thesis

Delft, 2020

Thesis committee: **Prof. Dr. AV. Metrikine**
Dr. Ir. K.N. van Dalen
Dr. J.M. Barbosa
Drs. Wybo Gardien, daily supervisor
Ir. A.B. Faragau, daily supervisor

سَنُرِيهِمۡ ءَايَٰتِنَا فِي ٱلۡأٓفَاقِ وَفِيٓ أَنفُسِهِمۡ حَتَّىٰ يَتَبَيَّنَ لَهُمۡ أَنَّهُ ٱلۡحَقُّۗ أَوَلَمۡ يَكۡفِ بِرَبِّكَ أَنَّهُۥ عَلَىٰ كُلِّ شَيۡءٖ شَهِيدٌ

“We will show them Our Signs in the universe, and in their own selves, until it becomes manifest to them that this (the Quran) is the truth. Is it not sufficient in regard to your Lord that He is a Witness over all things?”
Quran [41:53]

Contents

Abstract

Railways and other sources of environmentally induced vibrations often lead to annoyance and sometimes property damage. In this framework, transition zones are deemed as the most sensitive locations on the railway track, especially to high vibrations and impact loads. This causes high maintenance costs and is often very annoying, as the availability of the track gets limited during maintenance processes. One of the main reasons of this problem is the stiffness change of the railway supporting structure which is sometimes abrupt. This thesis will shed some light on the factors playing roles in altering the vibration intensities in level crossings. Moreover, the effects of these factors on ground vibrations will be highlighted. Further on, a model is presented which incorporates all these parameters. This model can be used to predict the change in ground vibrations in level crossings.

The objective of this thesis is to determine the influential parameters in terms of the response vibrations in the surroundings of railway tracks. On that account, following an in-depth literature study, and based on the analysis of the measurements performed at Movares, it was suggested to investigate three factors being the ambient temperature effect, the hanging sleeper scenario and the inhomogeneity of foundation and analyze their impacts.

The in-situ measurements illustrated a correlation with temperature, where the vibrations are amplified during hot periods and in the summer season. Besides that, the reports indicated the presence of the hanging sleeper scenario, where the suspension between the rails and the foundation is no longer active. It was also reported that locations with inhomogeneous foundations experience higher vibrations than those with quasi-homogeneous foundations. On those grounds, it was decided to study the effects of the hanging sleeper scenario, the ambient temperature and the presence of a slab-track crossing on the track.

A complete vehicle/track/soil numerical model has been used in the parametric study in order to assess the factors affecting the response vibrations induced by trains and to quantify their impacts. Along with that, the numerical results have been validated, to some extent, with analytical results. More specifically, the steady-state response obtained with both approaches are compared present a good agreement.

The results exhibit that the hanging sleeper phenomenon has a substantial effect on the vibrations. Furthermore, the existence of a level crossing (representing a foundation inhomogeneity) proved to be of significance as well. Lastly, the ambient temperature possesses a limited impact which could turn severe in extreme conditions.

Acknowledgements

After many months of commitment, persistence and dedication, it is wonderful to share the results of this hard work. Working on this thesis research, I did not only learn a lot, but also acquired huge technical and analytical skills. On a personal level, I learned new things about myself and massively improved my interpersonal skills. The beginning is always the hardest, but with the right people around it is possible to get through all the difficulties.

This thesis would have not been possible without the contribution of many people. If I have forgotten any names, please forgive me and be sure that I am quite appreciative of your assistance.

Wybo, no matter how much I thank you, it will not be enough. You did not just teach me a load of stuff in modelling, but also helped me improve my technical abilities. Your insight, knowledge and modelling experience were indispensable to this research. You have been like a rock to me during my hard times with the model. I really do appreciate your commitment and preciseness which are unmatchable. Thank you for your guidance throughout the course of this research.

Andrei Faragau, you are not only a magnificent supervisor and an incredible researcher, but also a good friend. Apart from that, your intelligence is beyond imagining, and your critical thinking and profound knowledge helped a lot in this research. Not to mention that our bi-weekly meetings kept me on track. Having worked with someone like you is a pleasure. Special thanks to you for your time and dedication.

Karel, you have that amazing way of simplifying problems, decomposing them into simple elements and showing how they fit together into a whole. Beside everything else being gorgeous, that made it particularly compelling. Maybe that is one of the reasons why structural dynamics became one of my favorite subjects. Thank you so much for your time and devotion.

Joao, your presence in this research was particularly valuable. Having an expert like you by my side was really comforting, but on the other hand also very exciting. I would like to thank you for your involvement.

Andrei Metrikine, it has been a privilege to sit in front of you in the lecture room and to be eventually one of the graduate students in your team. Your way of thinking and the style of explaining during the lectures has been wonderful. Turning the lecture into an internal challenge were everyone was spirited, that was quite unique. Thank you very much.

Herke Stuit and team dynamics at Movares, it was very nice working side by side with you in the office. Not only was it enjoyable, but also instrumental for me as I learned much during my tenure at the office. Thank you all for the nice talks we had and your advices that were always precious to me. Special thanks to Niels Lommers and the analysis team for helping me with the measurements analysis. I wish you all the best, and maybe our ways will meet again in the future.

My friends and mates, our time together has always been nice. We were always around for each other, and that is what made everything cheerful and easy. Thank you all for everything. Also many thanks to Ibrahim Koolstra for reading my report and providing constructive feedback.

Finally, I would like to thank my family, including my father Mahmoud Ellithi, my mother Reda Emara, my sisters Marwa and Salsabil, and my brothers Omar and Ahmed, for everything. Their endless support, infinite confidence and unconditional love were always very vital to me during the hard times.

Above all, I wish to praise Allah, the Almighty, for granting me determination, strength and resilience throughout this study journey, and giving me the chance to crown it all with this research. Alhamdulillah.

Enjoy reading!

Mohamed Ellithi
November 2020, Delft

1. Introduction

In this chapter a short introduction of the thesis project is presented, and then the problem statement is defined. Consequently, the research objective is emphasized after being divided into sub goals which will be addressed all in succession. Afterwards the research methodology is laid out in a chronological order. Finally, an outline is included to provide the reader foresight through the thesis.

1.1. Background

Traffic in general, railway traffic in particular and other sources of environmentally induced vibrations often lead to annoyance and sometimes material and geometry damage. Nevertheless, the severity of the situation remains dependent on the properties of the supporting structure, amongst others the stiffness. And due to the discontinuity of the supporting structure, the stiffness is always variant.

Transition zones are the most common example where the properties of the supporting structure vary with space, especially the stiffness. They can be defined as the limit zones between different track structures such as tunnels and viaducts, or where there is a change from conventional track to slab track, just to name a few. Level crossings are considered one of these transition zones. It is worth mentioning that there are more than 2,400 level crossings in the Netherlands according to ProRail, which is seen as a huge number in such a small country[1]. These zones are more susceptible to dynamic loads (and especially vibrations) which is troublesome and leads to quality deterioration.

Mitigation measures can be used to reduce these vibrations or minimize their impact. One of these measures is ShimLift which is a product of Kampa Rail and was applied by Movares in collaboration with Bam Rail. The ShimLift is a type of synthetic wedge that is placed between sleepers and rails, which raises the rail to the right level, while the sleepers continue to provide good support. By installing a ShimLift just before a level crossing, a better connection is made between the track and level crossing, potentially reducing vibrations from passing trains. The only issue is that in some cases it does not deliver sufficiently good results[2].

Taking into account the number of level crossings only in the Netherlands, and considering the surroundings, it is imperative that we take this field seriously. It is a matter of significance to be able to predict the vibration intensities in these areas and far more appreciated is to be fully prepared beforehand. This can trigger priceless social and economic improvements in the industry and can boost the sustainability level.

---

1 M. van Gompel, "Netherlands converts unprotected level crossings." *Railtech.com*, January, 2019.

2 M. Zasiadko, "Experiment with anti-vibration solutions on Dutch rail route successful." *Railtech.com*, February, 2019.

1.2. Problem statement

Since the onset of railways there have always been complaints of house vibrations due to train passage. And over the past years, railways have evolved much to become one of the most advanced and fast developing departments of transportation. In the wake of this progress, ground vibrations turned to be one of the most interesting engineering problems.

Meanwhile, the system of modern railways has been prone to high range modifications in terms of train weight, train speed and wagon axle load. This will certainly have its reflections in regard with the response and vibrations. Nevertheless, the ground vibrations caused by railway traffic are not everywhere the same as high. But when it exceed the acceptable level, it can prove costly in terms of both economic and social sides. The aim of this thesis is to shed some light on the reasons leading to differences in the intensities. This comprises the investigation of several parameters and the evaluation of their effects. This may provide a frame of reference for the design process in the future and pave the way for further research to resume.

1.3. Objectives and sub-goals

The main focus here lies on the ground vibrations associated with traffic. The impacts of these ground vibrations as mentioned before are highly priced on both the social as well as the economical perspective. For these impacts to be contained there is a need for models that can provide sufficient predictions about the intensities of these vibrations. With these predictions, measures could be taken to prevent or at least mitigate the upcoming effects. Two approaches could be used here, models be based on Finite Element Analyses or analytical models. Therefore, all the related parameters should be understood and analyzed thoroughly.

The main objective of this research is therefore to highlight the factors affecting the environmental vibrations in neighborhood of railway tracks. This includes the analysis of the acting load on the structure along with the foundation underneath and the response.

The sub-objectives can be elaborated in the following manner:

1) How far does the existence of a level crossing affect the environmental vibrations around railway tracks?
2) Is it possible to check the effect of the hanging sleepers scenario, also known as “blinde-vering”[3] and furthermore the option of ShimLift applications?
3) How to track the influence of (ambient) temperature on the railway tracks and vibration intensities?

[3] Blinde vering is a Dutch expression for the hanging sleeper scenario when the suspension or the connection between the rails and the foundation is totally separated.
J. Bos and J. Jansen “ShimLift.” *cdn.movares.nl*, April, 2017.

1.4. Approach and strategy

The research method can be overviewed in a number of stages:

1) A literature study is performed in order to collect comprehensive knowledge regarding railway tracks and level crossings and the potential factors to impact the response of the structure.
2) A model is developed with the capacity to incorporate all these different influential parameters.
3) A parametric study is carried out with the aim of evaluating the effect of these parameters.

1.5. Outline

In chapter 2, background information is collected regarding environmental vibrations and potential parameters of influence.

In chapter 3, a proper layout is given over the models used in this research. Consequently, a model validation is performed in chapter 4.

In chapter 5, some in-situ measurements and collected data are reviewed and discussed.

In chapter 6, the modelling process is addressed and the results are presented simultaneously.

Finally, the main conclusions and recommendations of this study are provided in chapter 7.

2. Background information

For the sake of having a sufficient preliminary understanding of the vibratory problem and the factors that come to play, some background information are collected. The different items are classified in three different categories; vehicle, track and soil. Afterwards, each one is addressed shortly. Some numerical in-situ / model results are included in order for clarity. For further information one can refer to ((Kouroussis, 2012); (Paul de Vos, 2017); (P. Alves Costa, 2012); (Aires Colaço, 2015)) or other related textbooks.

2.1. Vehicle parameters

When a train moves on a track, it generates vibrations and noise in the neighborhood. The vibrations induced in the vicinity are highly dependent on train parameters. Its type and subsequently the mass and speed. In the following sections, these items will be discussed briefly.

2.1.1. Vehicle type

There is a multitude of train types, and each with different properties. Variations in the mechanical and geometrical properties of trains mean that they generate different levels of ground vibration. Bearing in mind these being the source of excitation, a proper suggestion would be to take a closer look at these dissimilarities. They could be divided into three categories:

The first category is the Inter City Passenger Train group. This group includes all the intercity trains like ICM, ICR and ICNG along with the VIRM and the SPR. The ICR train is powered by electric locomotives while the rest are all trainsets. Another considerable difference to be mentioned here is the schedule frequency. The high vibration levels are normally created by means of the locomotives.

The second category is the High Speed Passenger Train group. This includes the German ICE, the French TGV, and the Swedish X2000. These trains have the potential to induce immensely high levels of ground vibrations. And this will be further discussed later.

The third category is the freight Trains. These trains are not all very similar and they are powered by either diesel or electric locomotives. They usually differ in length, number and size of locomotives, but mainly the number of heavy loaded cars.

It is worth mentioning that these types of trains vary in several characteristics. For instance, the axle load, the wheel diameter, the wheels being flat or worn, the suspension properties, the masses and the speed. Apart from that, the frequency is of noticeable relevance as well. These factors are estimated to give rise to differences in the ground vibration levels and some of them will be studied later.

Figure 2.1 ICM Train (Intercitymaterieel, n.d.)

Figure 2.2 ICR Train (typeicr, n.d.)

Figure 2.3 ICE Train (Intercity-Express, n.d.)

Figure 2.4 VIRM Train (z11307, n.d.)

Figure 2.5 SPR Train (Sprinter, n.d.)

Figure 2.6 ICNG Train (not in-service yet) (ns-icng, n.d.)

2.1.2. Vehicle mass

Train masses can be categorized into three sorts: the first one is the car body, the second one is the semi-sprung mass and the third one is the unsprung mass. The various types of trains mentioned before all differ with respect to these masses. Therefore it would be helpful to check the effects of these differences.

Initially, the car body was tested by (P. Alves Costa, 2012). In his research, he showed that the car body does not affect the dynamic interaction forces. The other two sorts have been analyzed by (Aires Colaço, 2015) amongst others in order to determine their influences. Doing that, he run a large number of simulations enough to better quantify these effects.

For clarity reasons, a graphical representation is included to distinguish the train elements:

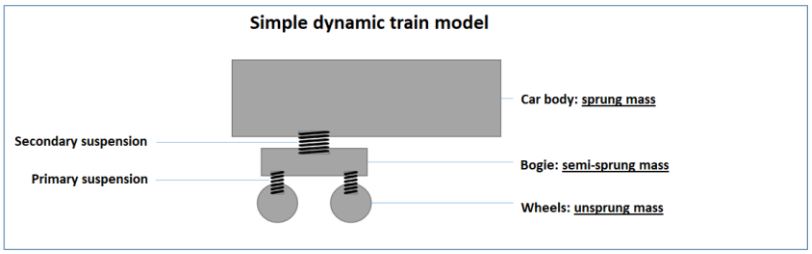

Figure 2.7 Train elements

According to the results, the unsprung mass does not produce a substantial consequence in the close vicinity of the track, as the response is then dominated by the quasi-static excitation. Nevertheless, this is not the case when moving further from the track, as then the dynamic excitation mechanisms become more relevant. So, the further the distance is from the track, the more effect is noticed owing to the unsprung mass. A view of his results is showed here below:

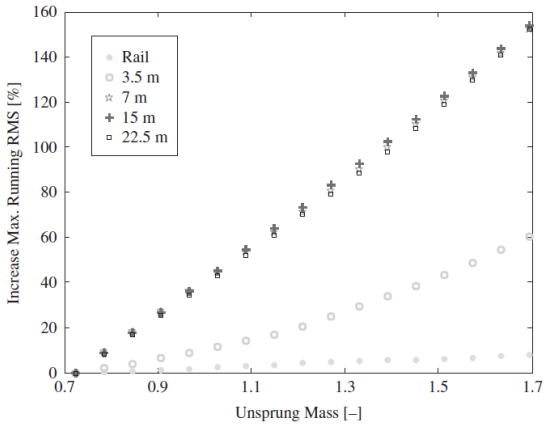

Figure 2.8 Velocity RMS vs Unsprung Mass (Aires Colaço, 2015)

Moving forward, the effect of the semi-sprung mass was then tested. (Aires Colaço, 2015) barely found any correlation between the changes is mass. A negligible effect was observed on both the quasi-static and the dynamic excitation. Likewise, almost no impact on the vibration level was found. In view of this, he concluded that the semi-sprung mass affects the response far lesser than the unsprung mass. Some of his results are included here as well.

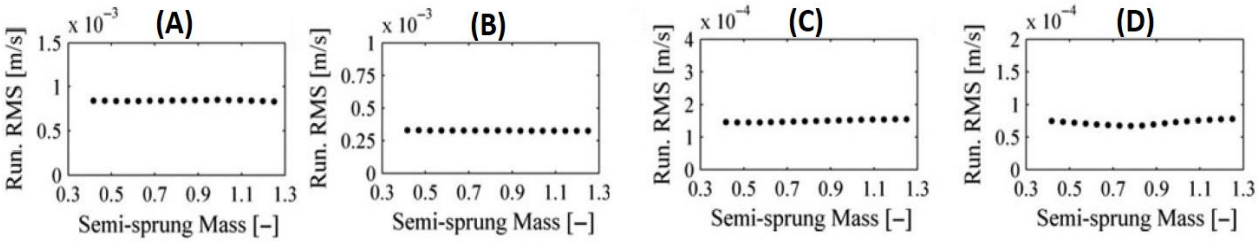

Figure 2.9 Velocity RMS vs Semi-unsprung Mass (Aires Colaço, 2015)
(measured (A): 3.5m from the track, (B): 7.0m from the track, (C): 15.0m from the track, (D): 22.0m from the track)

In his simulations, (Aires Colaço, 2015) used a six carriage train model with a total length of 158.9 m and he maintained a constant train speed of 212 km/h. He checked velocity vibrations and represented the results using the RMS value. Root Mean Square Amplitude (RMS) is the square root of the average of the squared values of the signal. It is numerically equal to the square root of the average of the squared value of amplitude. To calculate this value, the instantaneous amplitude values of the signal must be squared and then these squared values are averaged over a certain amount of time. This amount of time should be at least one wave period of the signal for the sake of getting a correct value. The squared values are all positive, and consequently their average as well. After that, the square root of this average value is the RMS value. The RMS value is the most common value used when a single value is wanted to describe the level of a dynamic signal.

It is worth mentioning that the TRAXX locomotive possesses the maximum mass values and with major differences than the others. Moreover, it has an unsprung mass value which is more than 1.5 times higher than of any other locomotive. That is why it is proper to shed some light on this later on.

Figure 2.10 TRAXX Loc (Bombardier_TRAXX, n.d.)

2.1.3. Vehicle speed

Train speeds have now increased beyond 360 km/h but here in the Netherlands it is restricted to a maximum value of 300 km/h. And as mentioned before, different train types exist, from which each type has its own running speed. For instance, the HSL and ICE can run up to 300 km/h, while the SPR, IC and TRAXX are limited to a 140 km/h speed. And finally, the freight trains may have a speed that varies from 80 to 100 km/h.

It is relevant as well to highlight that a major part of the country is covered with soft soil. Peat, organic clays, soft marine clays and silt have a low wave velocity which is not serviceable as railway foundation. These types of soil are particularly susceptible to excessive vibration from high-speed trains. This is very problematic and annoying. Moreover, it can also be dangerous, as it may lead to degradation of the embankment and foundation soil and fatigue failure of rails (Amir M. Kaynia, 2000).

So, train speed is a significant parameter that influences the response and therefore the vibration level. (Md. Abu Sayeed, 2016) investigated that effect along with the critical, sub-critical and super-critical speed and obtained astonishing results. At low speeds, the response due to the dynamic load is quasi-static; more specifically, the response relative to the moving load is very similar to the response obtained by a stationary load. When the velocity increases, the response caused by the moving load differs from the response caused by a stationary load. Furthermore, as the load velocity approaches the critical velocity, the response is greatly amplified.

2.2. Track parameters

The track support system is the first element to experience the load, and thus one of the major components in determining the levels of ground vibrations. Whether a (conventional) ballasted track or a slab track and the control system like the fasteners, pads, mats etc. all play a role in transferring the load and response. In the next sections, some items and relations are highlighted.

2.2.1. Rail and sleeper mass

Wooden sleepers has been common for a very long time, but recently concrete ties became popular as well. Meantime steel sleepers are also used, but not as widely as wood or concrete sleepers. Inter alia, this is related to damping which is relatively lower than in wood and concrete.

The influence of changing the sleeper mass along with the rail mass on the ground vibrations has been studied by (Kouroussis, 2012). In his model he hardly detected any change in vibrations as a consequence. After sufficient research he expressed that, neither the sleeper mass nor the rail mass do influence the maximum track deflection and thus the environmental vibrations.

Even though the mass and the flexural stiffness of the rail are related, it can be noticed that the rail mass does not affect the track deflection but conversely, the flexural stiffness does.

2.2.2. Track flexibility

The stiffness or the flexibility of the track is considered one of most decisive parameters influencing the environmental vibrations. It determines the track deflection shape and magnitude which (together with the ground self) govern the ground vibration intensities.

The flexibility of the track is determined by the rail, the rail pads and the ballast flexibilities, and of course the sleepers spacing as well. Although the variation of sleeper spacing is limited, the other parameters are all tested by (Kouroussis, 2012) in his model where he found out that the velocity vibrations in the vicinity diminish with a flexible track. Despite the fact that the flexibility leads to higher deflections, it is observed that it also result in lower velocity vibrations.

2.2.3. Rail and rail pads

It is relevant to highlight that when a train moves on a rail which is already vibrating (due to some previous loads/trains), this will affect the propagation of waves away from it and consequently the environmental vibrations.

Damping along the supporting system is a very significant parameter for the track as it determines the vibration's decay along the rail. It happens consequently by means of transmitting the energy away from the excitation point through the rail beam. This can be a result of two reasons, losses due to the elastic fastening system i.e. rail pads, and energy transmitted away into the sleepers and furtherly to the ground.

The rail pad stiffness is very effective in terms of the damping of the rail and the degree of coupling between the sleepers and the rail. For soft rail pads the sleepers are isolated from the rail vibration, and that is why the vibrations propagate relatively freely through the rail. In contrast, for stiff pads a good coupling with the sleepers is formed and thus, the sleeper is also vibrating, but the rail vibration is relatively less.

After sufficient investigation, (Thompson, 2010) proved that using stiffer pads leads to high decay rates in the rail for much of the frequency range.

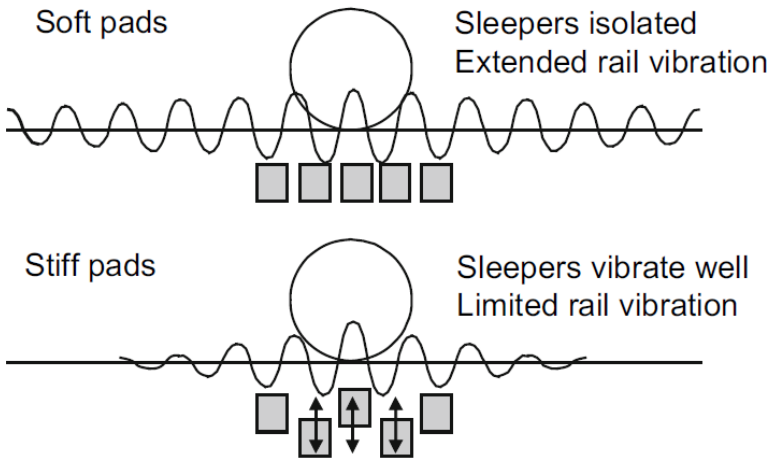

Figure 2.11 The effect of rail pad stiffness on rail vibrations (Thompson, 2010)

2.2.4. Track irregularity

The track irregularity and roughness play a significant role in the transmitted environmental vibrations, amplifying the effect of the passing axle load. This means that the roughness can lead to impact loads and collisions between the train and the rail. More importantly, the vehicle speed controls to a large extent the effect of track irregularity on the environmental vibration intensities along with the vehicle dynamics (Kouroussis, 2012).

2.3. Soil / foundation parameters

Soil properties are well known of a remarkable influence on the levels of ground vibrations. Within the most important factors are the stiffness and the internal damping of soil, but also the mass density of soil. More importantly, the layering of soil, the depth to bedrock (which is not well known in the Netherlands) and the ground water table can have significant effects on the vibration energy and its further propagation.

The stiffness of the soil among other properties, is supposed to determine the level of vibrations that are generated by means of the rail traffic. The vibrations travel through the ground in the manner of waves, and that could happen in different forms. The most essential three forms are namely the surface wave, the longitudinal wave and the transversal wave. They are swiftly introduced here in a small preview.

The surface waves also known as Rayleigh waves are named after Lord Rayleigh who first considered the waves propagating along the surface of an elastic half space. These waves occur at the surface of the soil and strongly decrease with depth. Particles have a circular movement comparable to waves in water. This type of wave is considered the utmost important one in this context, as the load (moving train) takes place on the surface. A graphical representation of it is shown below:

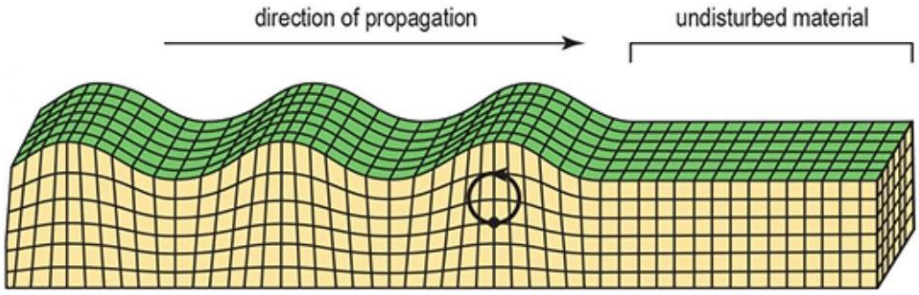

Figure 2.12 Rayleigh waves (Paul de Vos, 2017)

The longitudinal waves also known as primary or pressure waves (P waves). These maintain the highest propagation velocity of the three and have the longest wave lengths. These waves in our case propagate mainly downwards into the medium. The propagation velocity depends on the density of the ground and the dynamic shear modulus. With higher densities a higher propagation velocity occurs. A graphical representation of it is shown below:

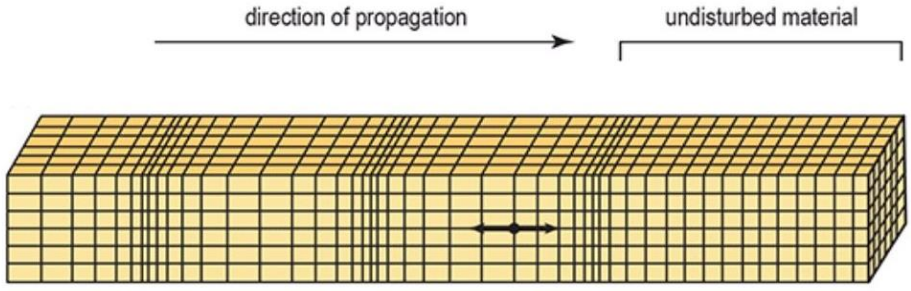

Figure 2.13 Pressure waves (Paul de Vos, 2017)

The transversal waves also known as shear waves (S waves). The particles here move perpendicularly to the (train) movement direction as shown in the figure below. The propagation velocity depends on the density of the ground and the dynamic shear modulus. With higher densities a higher propagation velocity occurs.

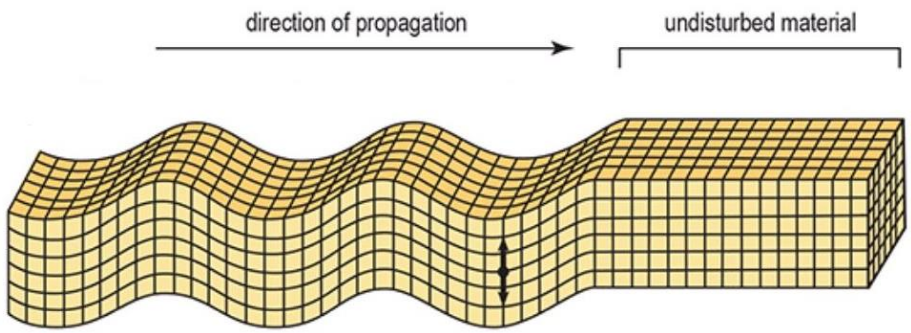

Figure 2.14 Shear waves (Paul de Vos, 2017)

Extremely large differences can exist between the different soils in terms of these wave velocities. For example, the maximum value of the shear wave velocity could reach 275 m/s while the minimum yet be round 50 m/s. Even vaster variations are observed in the values of the pressure wave velocity like between 1761 and 286 m/s (Paul de Vos, 2017). This underlines how diverse the soil properties could be and therefore their performances. The next paragraphs addresses these properties.

2.3.1. Shear modulus and Young's modulus of soil

Both quantities describe the stiffness of the soil. For instance, the Young's modulus E in general describes the material response to uniaxial stress in the direction of this stress. Secondly, the shear modulus G describes the material response to shear stress. The shear modulus is also dependent on Poisson's ratio which is relevant here as well. Accordingly, each soil type has a different stiffness which makes it a characteristic value.

As previously mentioned, soft soils such as clay or peat covers a substantial portion of the country. These types of soil possesses poor conditions amongst others having a low wave velocity. Having a low wave velocity impose constraints like decreasing the operational speed in order to avoid large stresses and strains. In some situations the train speed can be limited to a maximum of 140 km/h or even lower. As a consequence, engineers started to think of alternatives like soil improvement through soil replacement or soil stiffening.

One of the researches in this area belongs to (C. Bayındır, 2018). He analyzed the effect of increasing the soil stiffness on the response of moving trains. He showed that increasing the vertical stiffness of the foundation can effectively decrease the vibration levels. More particularly, doubling the stiffness results in 25% reduction in RMS velocity and RMS acceleration levels. Furthermore, increasing the stiffness by a factor of 5 results in 60% reduction of the levels. And some of his results are presented below.

For the sake of clarity, (C. Bayındır, 2018) modelled the railway as a Winkler foundation with rail pads, and consistently increased the vertical stiffness in the foundation.

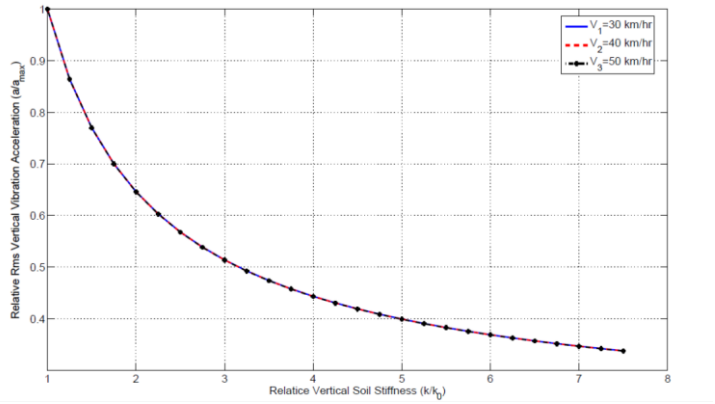

Figure 2.15 RMS velocity vs Soil Stiffness (C. Bayındır, 2018)

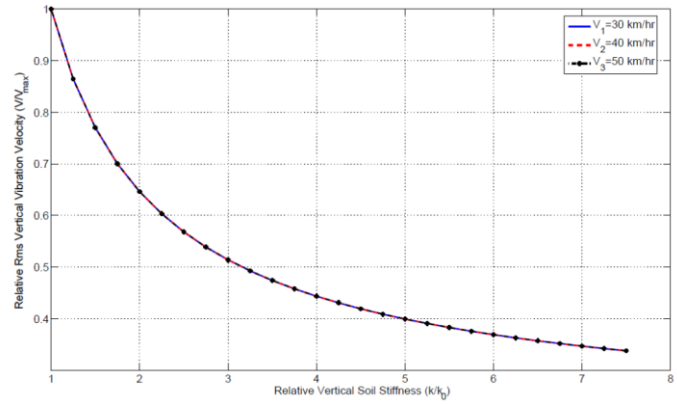

Figure 2.16 RMS acceleration vs Soil Stiffness (C. Bayındır, 2018)

The dynamic shear modulus of soil denoted as G is a significant characteristic of it. As mentioned earlier, It does not only describe the stiffness of the soil but also determines its wave velocity. So, it was no surprise what people showed through research. Amongst others, (Kouroussis, 2012) managed to analyze the shear modulus effect on railway environmental vibrations by means of a numerical model. He indicated that by means of increasing the shear modulus, the vibrations decline. Some of his results are shown here.

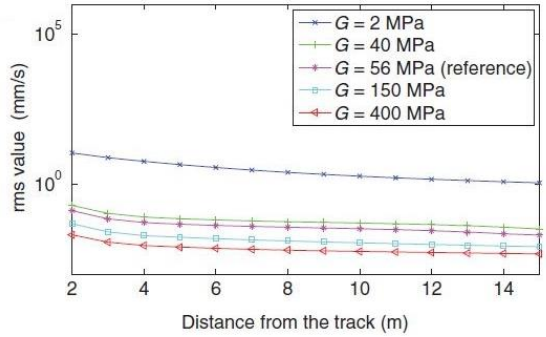

Figure 2.18 RMS velocity vs Shear Modulus (Kouroussis, 2012)

2.3.2. Damping

Damping could be defined as the loss of energy within a vibrating or a cyclically loaded system, possibly in different forms as heat. It is commonly used in geotechnical engineering as a measure for energy dissipation during dynamic or cyclic loading.

Two types of damping can be classified. The first one is the internal damping which includes the energy dissipation within the material itself, mainly due to microstructural mechanisms. In soils, this happens by means of many reasons including inter-particle sliding and friction, structure rearrangement, and pore fluid viscosity (A.K. Ashmawy, 1995). This type of damping is a material property and that is why is known as material damping. The other type of damping is denoted as the external damping which comprises energy losses within a structure or a structural member due to factors other than internal friction. This type of damping is referred to as system damping.

In this context, the material damping is rather relevant. The various kinds of soils all diverge in characteristics and consequently possess unequal damping values. However, soft soils maintain higher material damping. Nevertheless, in general damping is of a considerable significance in terms of decreasing vibrations and avoiding a very high-amplitude response. (Kouroussis, 2012) studied that in his three-dimensional model and showed that the vibratory levels diminishes with increasing damping. A preview of his graphical results is included as well.

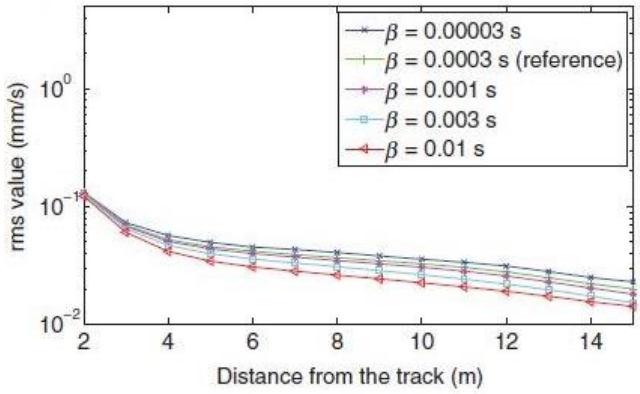

Figure 2.17 RMS velocity vs Rayleigh Damping β (Kouroussis, 2012)

2.3.3. Groundwater table

A special feature of soil is that water could be present in its pores. When that happens the soil properties are then no longer as before. The stress transfer in the soil is heavily affected by this water in the pores. In addition to that, when this water flows relative to the soil particles, it produces friction stresses between the fluid and the solid material (Verruijt, 2017). What is even more crucial here is that the water table is commonly expected to have substantial effect on ground vibrations. But unfortunately, it is an unsteady environmental phenomenon which implies that it is hard to be controlled.

2.3.4. Other associated parameters

Aside from the mentioned parameters, other essential soil parameters also exist. For instance, the mass density which influences the wave velocity in it. As mentioned earlier, a decisive parameter in the vibratory problem is the wave velocity of the medium which is directly related to the mass density through the upcoming equations (W. Gardien, 2003):

$$C_p = \sqrt{\frac{G}{\rho} * \frac{2(1-\nu)}{(1-2\nu)}} \qquad \text{eq. (2.1)}$$

$$C_s = \sqrt{\frac{G}{\rho}} \qquad \text{eq. (2.2)}$$

$$C_r \approx 0.9 * C_s \approx 0.9 * \sqrt{\frac{G}{\rho}} \qquad \text{eq. (2.3)}$$

Respectively, eq. (2.1) represents the pressure wave speed, eq. (2.2) the shear wave speed and eq. (2.3) the Rayleigh wave speed. Whereas the soil shear modulus is denoted by G, the mass density by ρ and Poisson's ratio by ν.

Another soil characteristic to be highlighted is Poisson's ratio which may be described as the deformation of a material in directions perpendicular to the direction of loading. As seen above, the wave velocity is yet dependent on it. Furthermore, (Kouroussis, 2012) demonstrated the presence of a slight link with the vibratory problem and that is presented in Figure 2.19.

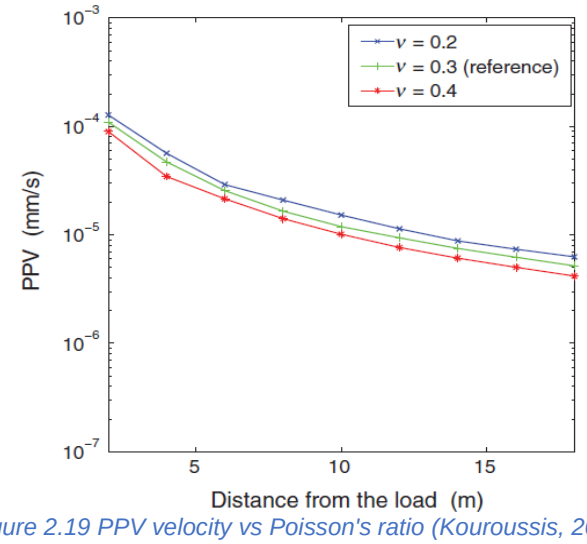

Figure 2.19 PPV velocity vs Poisson's ratio (Kouroussis, 2012)

Nevertheless, due to some limitations in this research, not much attention will be drawn on this relation.

2.4. Temperature

The temperature generally indicates the direction of the flow of heat energy which is namely from the hotter body to the colder body. The soil temperature is related to the difference between the absorbed (heat) energy and the (heat) energy lost from the soil. It fluctuates annually and daily, as a result of changes in air temperature and solar radiation (Onwuka, 2018). These two parameters both correlated to the weather which varies periodically. It is also important to note that these variations does not always take the same pattern. In some situations it could follow a completely different course. In the figure below, (Sun, 2016) made a distinction between two different cases. On the left side a representation of a typical day is shown. On the right side an out of norm day with a noon rain is shown. Additionally, he viewed the temperature of the pavement following these daily variations.

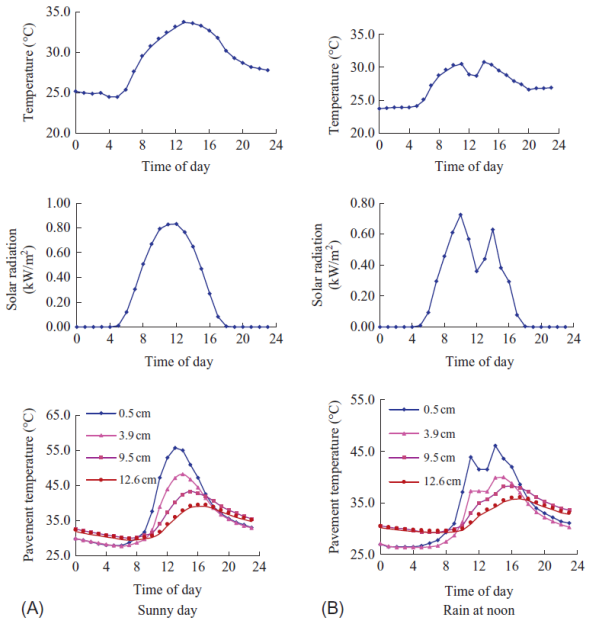

Figure 2.20 Variety of daily weather and pavement temperature (Sun, 2016)

As shown in the figure, the temperature of the pavement follows these daily variations. In his book, (Sun, 2016) stated that among other environmental factors like solar radiation and wind speed, air temperature is the most significant factor in pavement temperature distribution. Apart from that, even though the solar radiation happens only during daytime hours, it plays the main role in increasing the pavement structure temperature. In the interests of clarity, the different involved environmental factors are represented in the figure.

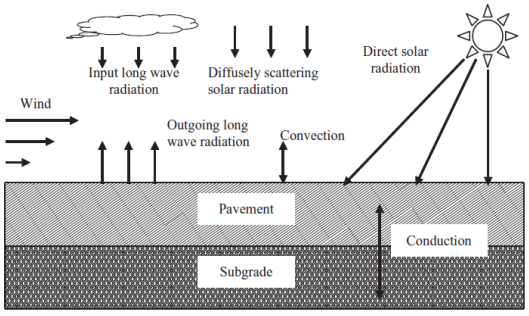

Figure 2.21 Environmental factors affecting pavement temperature (Sun, 2016)

On those grounds, the soil temperature varies seasonally and daily as a result. Merely the top layer gets involved in this duel, but still we keep in mind the fact that soil temperature is one of the important factors that influence soil physical and mechanical properties. This statement is discussed in the next paragraphs.

As a matter of fact, it is been established by many theoretical and experimental studies (Laloui and Di Donna, 2013); (C. Zhou and C. W. W. Ng, 2015) that the soil behavior is related to the temperature amongst others. Consequently, to better understand the thermal effect on soil behavior and to be able to foresee the ground movement and dynamic response of geo-structures, research has been conducted in this regard.

2.4.1. Temperature effect on soil stiffness

A series of cyclic tests were completed by (C. Zhou and C. W. W. Ng, 2015) to analyze the thermal and suction effects on soil stiffness. They developed a temperature- and suction-controlled system which made it possible to perform their experiments. They tested the temperature effects at three different suction levels (0, 30 and 60 kPa). At each suction level, three tests were completed at three different temperatures (20, 40 and 60°C). Hence, totally nine tests were carried out at four levels of cyclic stress.

When maintaining a suction level of 60 kPa, it was noted that the Young's modulus decreases by about 20% as temperature increases from 20 to 60°C. This is called thermal softening was rather explained before by (Laloui and François, 2008). When the temperature increases, the yield stress of unsaturated soil decreases which is very likely the reason behind the reduction of the Young's modulus. In Figure 2.22 below, the results of this test series are presented.

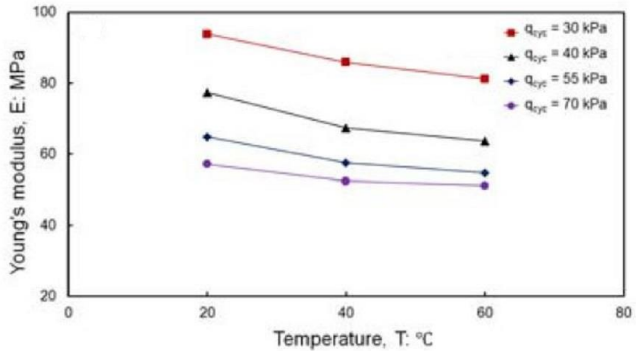

Figure 2.22 Young's modulus vs temperature (C. Zhou and C. W. W. Ng, 2015)

Following this, the next group of specimens were tested at a suction level of 30 kPa. No major difference than the previous ones was noted. Likewise, at this suction level, the Young's modulus also decreases consistently while the temperature increases. This has been illustrated in Figure 2.23 below. More importantly, no major difference than the previous relation is perceived.

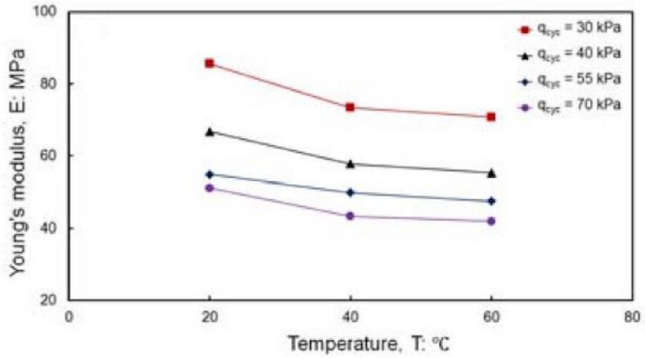

Figure 2.23 Young's modulus vs temperature (C. Zhou and C. W. W. Ng, 2015)

Finally, the last series of tests were conducted without including any suction on the specimens. Here the relation solely between the temperature and the Young's modulus was represented. It was identified at lower stresses (30 and 40 kPa) that, when the soil temperature increases from 20 to 60°C, Young's modulus increases by roughly 5%. In contrast, at higher stresses, Young's modulus gets reduced by the same percentage when rising the temperature. A graphical representation of this result is showed here below in Figure 2.24.

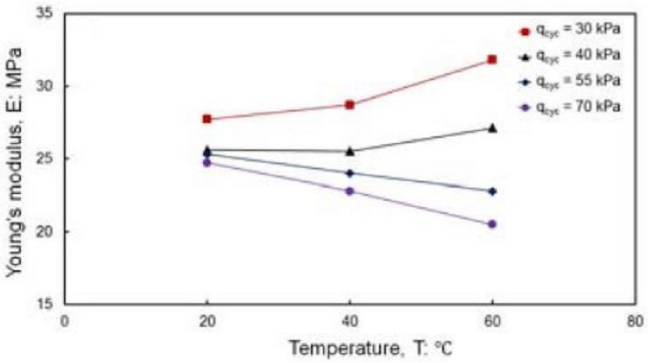

Figure 2.24 Young's modulus vs temperature (C. Zhou and C. W. W. Ng, 2015)

It can be realized from these tests that the thermal effects on the resilient modulus are more crucial in the presence of suction. Apart from that, in the absence of suction, the stress level is quite decisive.

2.4.2. Temperature effect on soil shear modulus

So far as it relates the thermal effects on the soil shear modulus, many tests were carried out by (C Zhou, 2015) and (B. Ghahremannejad, 2003) among others. Using temperature-controlled triaxial apparatus, and applying diverse tests, both of them managed to analyze the shear modulus of soil.

On one hand, (B. Ghahremannejad, 2003) drew attention to the saturated soil. Through his tests, it was found that, at the same strain, the shear modulus is consistently smaller at higher temperature. It should be pointed out here that this is valid for small strains.

On the other hand, (C Zhou, 2015) focused on the unsaturated soil. Various triaxial compression tests were conducted to investigate the behavior of the shear modulus. The tests were completed at two different suction levels (1 and 150 kPa). From the

results, it has been highlighted that for the same suction level, the shear modulus at a given strain is slightly smaller at higher temperature. This is clearly illustrated in Figure 2.25 below

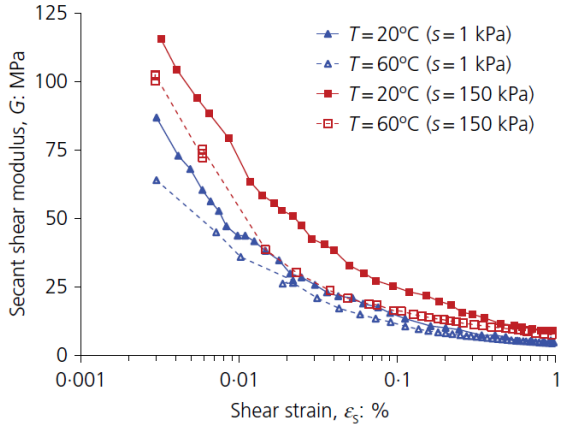

Figure 2.25 Shear modulus vs temperature (C Zhou, 2015)

Besides that, the shear stress-strain behavior was reviewed as well. It appears that the temperature has some implications on that as well. As presented in Figure 2.26 when the temperature increases the shear strength lightly decreases.

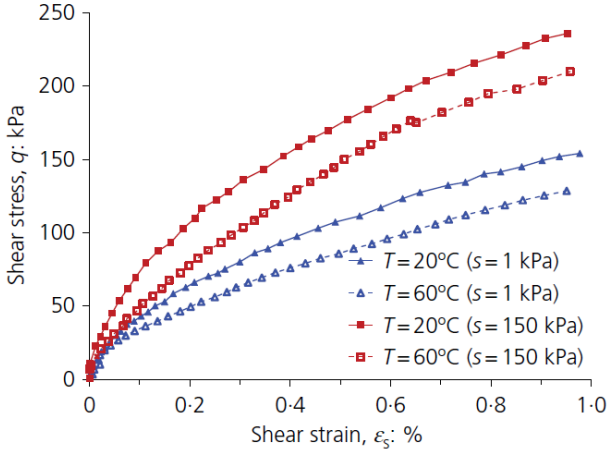

Figure 2.26 Shear stress-strain vs temperature (C Zhou, 2015)

2.4.3. Temperature effect on rail pads

The properties of viscoelastic materials like rail pads are sensitive to the temperature. This has been investigated earlier by (R. A. Broadbent, 2009). In his study, he used two samples of rail pad material, a studded natural rubber pad and cork rubber pad. In a temperature chamber the experiments have been performed and consequently the thermal dependence was determined. The analysis was done over a temperature range of -20 to 40°C. In the meantime, the shear modulus, stiffness and damping were continuously measured. The results are shown shortly in the figures below.

From the tests, it appears that the temperature has a considerable impact on the rail pad properties. As the temperature gets higher, the shear modulus of both samples

decreases. Furthermore, a pronounced decrease in stiffness and damping with increasing temperature is exhibited in both railroad materials.

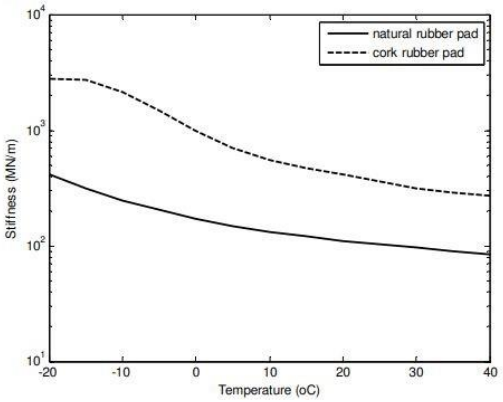

Figure 2.27 Rail pad stiffness vs temperature (R. A. Broadbent, 2009)

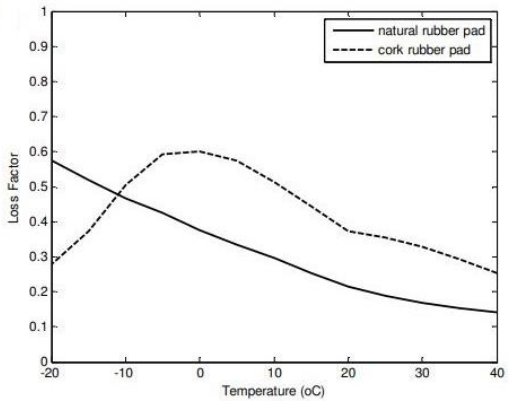

Figure 2.28 Rail pad damping vs temperature (R. A. Broadbent, 2009)

2.4.4. Temperature effect on the rail

There is no question that all modern rails nowadays are hot rolled steel. Overall, steel as a material has a strong dependency on the temperature. The temperature change does not only affect the mechanical behavior as an additional load, it also modifies all the material properties. This will be concisely discussed in the following paragraphs.

Railway steel contracts at low temperatures and expands at high temperatures (Rail_stressing, 2019). In extreme coldness, a length of continuous welded rail experience severe tensile stress. This stress can lead railway steel to fracture. By contrast, at extreme high temperature, the length of continuous welded rail could suffer compressive stress. This type of stress can cause a length of a railway to buckle laterally (sideways) as previewed below.

Figure 2.29 Rail Buckling (Railway Buckling, 2016)

As mentioned earlier, the temperature fluctuates seasonally and daily due to the climate change. But this is not the only reason increasing the rail temperature. According to research of the University of Birmingham (NetworkRail_news, 2019), it was concluded that on a warm day and in direct sunlight, the tracks can be 20°C warmer than the ambient temperature. In addition to this, the extra energy of a passing

train, and when multiple trains pass, all cause increasing the rail temperature. This implies that in extremely hot weather, it can rise up to more than 70°C. In such cases, the temperature effect on the rail properties may be significant.

Moving onward, when the rail temperature gets higher, rail deformation could take place. It is then important to note that if the rail is laterally constraint, it will deform vertically. This will result in vertical displacements in the rail which may also be identified as rail upwarping. This phenomenon was previously studied by (Juanjuan Ren, 2017). He maintained a Longitudinally Coupled Prefabricated Slab Track system and gave particular attention to the response under thermal loading.

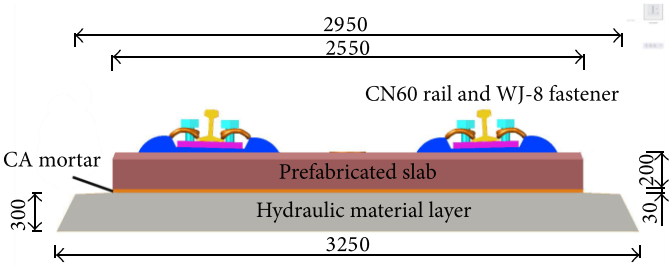

Figure 2.30 Longitudinally coupled prefabricated slab track system (Juanjuan Ren, 2017)

Using both analytical and numerical methods he could quantify the vertical upwarping of the track. In addition to that, he also analyzed the response and addressed the influence of different factors on that phenomenon. These results strongly demonstrate how influential the temperature can be on the track performance.

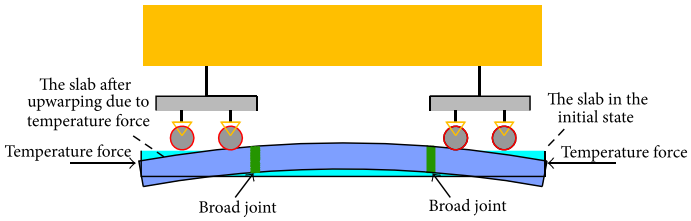

Figure 2.31 Track upwarping (Juanjuan Ren, 2017)

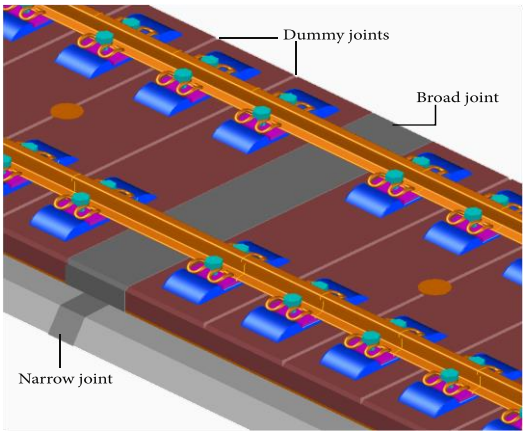

Figure 2.32 Track layout (Juanjuan Ren, 2017)

Ultimately, the fact that the temperature fluctuates frequently, indicates that the rail experiences cycles of cooling and heating. Without disregarding residual stresses, it becomes apparent that the function of the rails goes far beyond the train loads. Taking all this into consideration, gives a clear view how fatigue may happen and how the durability could be affected.

3. Model layout

In this chapter, a proper description is given for the numerical model used in this research. The analysis and the data presented here are outcomes of that model.

3.1. General

The numerical model comprises two main modules: one addresses the train loads on the track and the train-track interaction; the other considers the track-ground structure and the interaction between the foundation and the track. However, the two modules are not coupled, which implies that the response cannot influence the load induced by the train. The main aspects and assumptions of both models are described in the next paragraphs.

3.2. Train-track interaction

The train-track interaction and loading analysis is performed by a 1-D model called spoormodel. This model was originally constructed and developed at Movares. Herewith, several aspects of the dynamic behavior of the train moving on a track can be analyzed. The train is modelled using a multi-body formulation (as in Figure 3.1 below), while the total track body is simulated by a 1-D layered structure. The input is implemented in Ansys while the simulations are made by means of the generic finite-element program LS-Dyna.

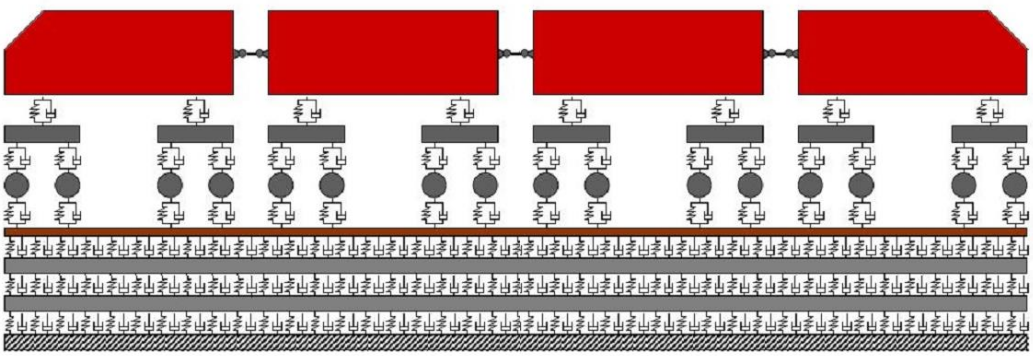

Figure 3.1 Spoormodel

In general, the model can be shaped as the user wishes through the input process which can be described in a few steps. Primarily, a model of the vehicle and the track construction can be built up in the Ansys program. That model which is built up in Ansys is an input file for the LS-Dyna program wherein the calculations are performed. Afterwards, and following these calculations, the results (like displacements, velocities, forces, stresses, etc.) are available and can be visualized in a post-processor.

First of all, general information about the simulation can be specified, for instance, defining element types, vehicle speed, duration of the simulation, interaction between track and vehicle and magnitude of time steps for the output. Regarding the interaction between track and train, it is possible to define a rail roughness function. In addition to that, a (lateral) wind load could be included in the problem just as well.

Secondly, data concerning the vehicle is specified upon which the model of the train is then formed. The geometry and material properties of the vehicle are then determined. Movares has a train database that includes several types of operating trains from which a certain train could be chosen with its typical properties. Besides, it is also possible to ultimately design another different train with the needed characteristics and parameters.

Thirdly, data regarding the track is specified upon which the model of the track is constructed. The geometry and material properties of the track can be assigned. It is possible here to identify the structure being a slab track, a conventional (ballasted) track or else. Additionally, the alignment could be selected being straight or curved. Moreover, any (abrupt) change in the foundation layers maybe modelled here as well.

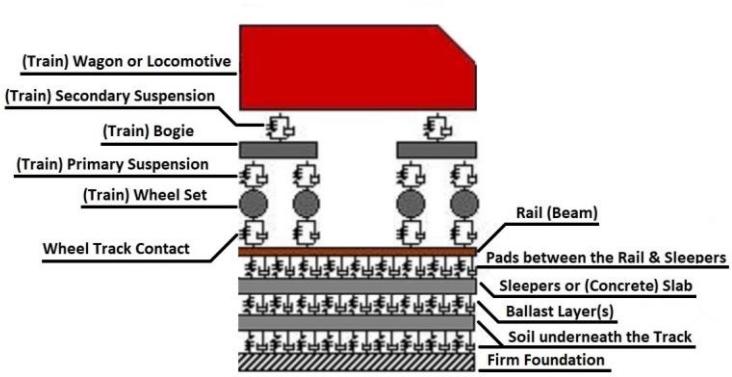

Figure 3.2 Model elements

As presented in Figure 3.2, the train is modelled as a mass-spring-damper system, concluding a car body, two bogies, four wheelsets, and suspension elements. This implies every vehicle having 14 DOFs, counting car body motions, bogie frames motions, and wheelsets motions.

The train-track contact is simulated by a linear spring connection being simplified by excluding the dampers because it is negligible at the contact between the wheel and the rail. The track is modelled in layers as seen in the Figure 3.2. The rail is represented by the upper Timoshenko beam, the rail pads by the spring-damper connection beneath. Afterwards, the fastening system is modelled by means of a beam if it is a slab, while point masses in case of sleepers. Then the ballast is accounted for by again a spring-damper connection. Finally, the soil is converted from a half space foundation into an elastic Timoshenko beam supported on visco-elastic footing by means of the track-ground model which is introduced in the next section.

One downside of this model is that it does not have the capability of fully describing all the interactions that actually take place. For instance the lateral (hunting) motion of train, and the movement of the vehicle parts relative to each other. But given the fact that the objective is more related to the environmental vibrations in the vicinity of the track, means that this limitation cannot be vigorous in this context.

3.3. Track-ground interaction

The track-ground analysis is performed by a 3-D model called GeoVib. This model was also originally constructed and developed at Movares. Through this model, it is possible to make predictions about vibration intensities, as a result of a vibration source. These predictions could be provided for any point in the terrain nearby the vibration source. Similar to Spoormodel, GeoVib is scripted in Ansys. Nevertheless, the computations could either be performed by Ansys or LS-Dyna. But in regards to complicated models, it is rather recommended to run the simulation in LS-Dyna, since the computation time will be shorter.

As highlighted above, the program is capable of calculating the vibration intensities in the ground for a large number of situations. Withal, it is possible to apply modifications to the source (load type), the soil structure (dimensions and properties) and the geometry. Geometry includes not only classical constructions like train-track structures but also road structures at ground level, tunnel constructions, or when the vibration source acts at variant heights like incase of foundation piles etc.

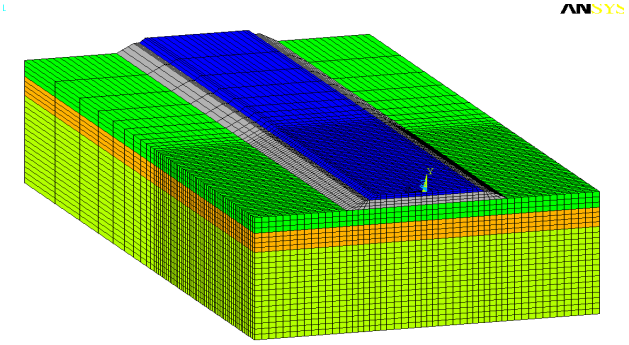

Figure 3.3 GeoVib model

After building up the model and before starting the computation process, the model can be previewed by means of Ansys. This step is optional and is used to check model build-up and meshing. Below in Figure 3.4, a model is previewed showing a track with embankments and a building (in green) in the neighborhood. It is clear that each ground layer has a different color as well as the surrounding reflection layers (bigger in size) in the far domain. Furthermore, the boundary conditions indicate that the model is restraint in the lateral direction due to symmetry. This intermediate step is handy as it facilitates the process and minimizes time-waste.

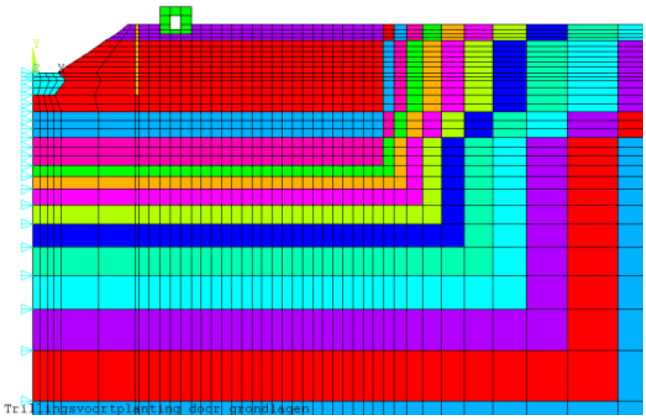

Figure 3.4 Model with embankments and ground layers

Furthermore, regarding the computation process, the model could be selected being a plain strain model or axi-symmetrical or 3D. For some situations, this need to selected carefully. However, in this research problem, it does not have a significant influence on the outcome.

It should just be pointed out here that in the version of Ansys used in scripting GeoVib, it is not possible to define infinite boundary conditions. This is further handled by means of damping layers which prevent reflections. And therefore, the results of the model are to some extent sensitive to reflections.

3.4. Combining both models

In the case of linear systems, the displacement of any track or structure can be calculated using the response of an impulse. This can ease the process, since with a single impulse response any desired load can be calculated over time. This is addressed in this sub-section.

Firstly, we run analysis with spoormodel and obtain the results for the contact forces between the sleepers and ballast. After that, we further on use GeoVib which accounts for all the layers up to the ballast layer, as seen in Figure 3.3. Bearing in mind here that the model in GeoVib is linear, implies that we can solve the problem using the Green's function method. As the Green's function relies on the principle of superposition, the solution to a linear system can be expressed as a convolution of the impulse response of the system with the prescribed force. The Green's function has the following form:

$$G(x, t; x_s, \tau)$$

This applies where x is the location of the receiver, x_s is the location of the source, t is the observation time and τ is the time of the excitation source.

In the spirit of this simplicity, it is relevant to highlight that the model in GeoVib is longitudinally translational invariant. This includes that the response of the system to impulse loads at two different location along the same longitudinal axis is the same, but shifted in time. This fact is indicated through the equation below:

$$G(x, t; x_s, \tau) = G(x, t - \tau; x_s, 0) \qquad \text{eq. (3.1)}$$

The contact forces in the track from the Spoormodel are prepared as the source excitation function: $F(x_s, \tau)$

These forces from Spoormodel are only applied at the surface of the ballast, and so, we don't need to find the Green's functions for all excitation points in the domain. This makes the process more computationally efficient.
Ultimately, when convoluting the Green's function with this (train) excitation function, the response to the $F(x_s, \tau)$ excitation load can be found. The displacement field along the same line can be derived through the following equation:

$$U(x,t) = \int_0^t \int_{-\frac{L}{2}}^{+\frac{L}{2}} G(x, t-\tau; x_s, 0) * F(x_s, \tau) dx_s \, d\tau \quad \text{eq. (3.2)}$$

Finally, for each point, the response due to all the different forces at different locations and different time moments will be integrated to get the total response. The load obtained from Spoormodel is only applied at the surface of the ballast, and so, we don't need to find the Green's functions for all excitation points in the domain. This makes the process more computationally efficient.

It is worth noting that for the level-crossing scenario, the level-crossing is modelled only in Spoormodel (when obtaining the loading function) and this is not modelled in GeoVib. The reason is because the system will not be translational invariant in the longitudinal direction, and therefore, the number of excitation points for which Green's functions that have to be obtained increases drastically, making the model very slow.

3.5. Final results

After combining both modules and accumulating their analysis, the final response is eventually obtained. In the postprocessing, it is possible for any given location in the terrain nearby the vibration source (moving train) to retrieve the vibration history. Displacements, velocities and accelerations could be displayed as a function of time or distance. Apart from these, forces can be checked as well. Spatial variations could be visualized with the aim of comparison. Over and above, it is possible to display results for different time moments in succession. An animation could be created to review the development along a certain time length. A proper initial representation for the model could be performed by animating the deformed mesh through time.

4. Model validation

Before working with models, it would be meaningful to check the correctness through a calibration or validation process. This will be provided in this chapter.

4.1. General system

The general system to be used in the validation is depicted below in Figure 4.1. It consists of an Euler-Bernoulli beam, visco-elastic foundation and a moving load. The model has an infinite length and is described by a positive upward coordinate system.

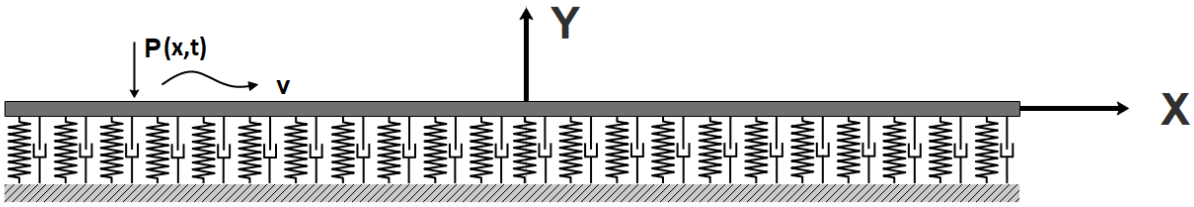

Figure 4.1 Infinite beam on visco-elastic foundation

The Euler-Bernoulli beam is a one-dimensional model describing a beam element. This represents the rails in our application. In so far as possible, the beam have been granted the same properties as the rails. Along with this, a number of assumptions hold in this derivation. The shear stiffness has been assumed maximum which involves no shear deformation. Nevertheless, this has been accounted for in the numerical model. Supplementarily, the rotational inertia of the beam has been neglected.

The visco-elastic foundation underneath the beam comprises a layer of continuously distributed springs and dashpots. This one-dimensional foundation model incorporates the behavior of the sleepers, the ballast layer and the subsoil. The properties of this layer corresponds the equivalent properties of all these layers. One assumption to be emphasized here is regarding the mass. This layer includes elements which entail that the foundation mass is neglected in this model.

The load is assumed to have a constant magnitude and the contact with the beam is continuous. Not only that, but also the velocity is held constant, and the system is assumed to be straight which suggests that the load has a uniform path.

The model is of an infinite length in spite of the fact that railway tracks actually have a finite length. Yet for engineering purposes, it is conceivable to be defined in such manner. Systems in general can be deemed infinite if the distance between the boundaries is large enough such that they do not influence the behavior of the system in between (Faragau, 2017).

The coordinate system is specified as in the figure above. The system has a stationary reference frame with a positive upward vertical axis. This conveys that the positive displacement of the system $\mathbf{w(x,t)}$ will point upwards.

4.1.1. Mathematical derivation

Now that the system is established and the coordinate system is defined, the next step is to start deriving the equation(s) of motion. The whole derivation including the equation of motion of the system is elaborated and discussed in Annex A. Thereby the equation of motion reads as follows:

$$\rho A\frac{\partial^2 w(x,t)}{\partial t^2} + EI\frac{\partial^4 w(x,t)}{\partial x^4} + C\frac{\partial w(x,t)}{\partial t} + Kw(x,t) = -P\delta(x-vt) \quad \text{eq (4.1)}$$

where ρ denotes the density of the Euler-Bernoulli beam, A the cross-sectional area and EI the bending stiffness. The distributed damping is referred to by *C* while the distributed stiffness by *K*. The forcing term can be observed in the right hand side where *P* represents the magnitude, *v* represents the velocity and δ is the Dirac-delta function.

In a more compact form, the equation of motion is restated below. The dot symbolizes a time derivative and the prime a space derivative. The function variables *x* and *t* are excluded from the equation as well for the sake of simplicity. Now it reads:

$$\rho A\ddot{w} + EIw'''' + C\dot{w} + Kw = -P\delta(x-vt) \quad \text{eq. (4.2)}$$

In order for obtaining the steady-state solution later on, it is convenient to divide the total system into two domains; the 1st domain represents the system behind the load $x < vt$, while the 2nd domain in front of the load $x > vt$. The load P will be included in the interface conditions.

$$\rho A\ddot{w}_1 + EIw_1'''' + C\dot{w}_1 + Kw_1 = 0 \qquad x < vt$$

$$\rho A\ddot{w}_2 + EIw_2'''' + C\dot{w}_2 + Kw_2 = 0 \qquad x > vt$$

eq. (4.3)

In the following picture both domains can be distinguished. Each domain has its own displacement field and described by an equation of motion as specified in eq (4.3). Now that the problem is clearly described, the next step is to derive the interface condition.

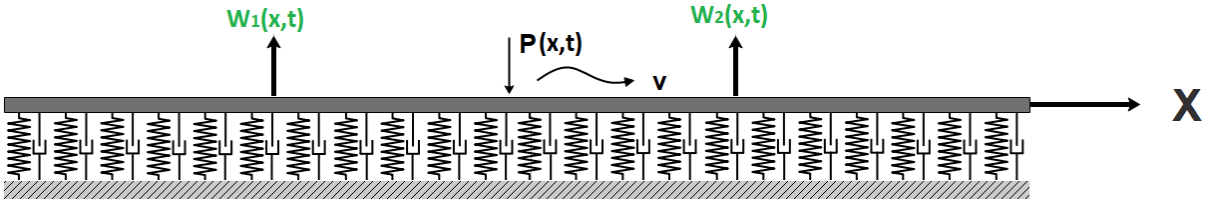

Figure 4.2 Infinite system with a moving reference frame coordinate system

For the sake of conciseness, as in eq (4.2), and through dividing on the bending stiffness, then the formulas in eq. (4.3) will read as follows:

$$\begin{aligned} &{w_1}'''' + \frac{\rho A}{EI}\ddot{w_1} + \frac{C}{EI}\dot{w_1} + \frac{K}{EI}w_1 = 0 && x < vt \\ &{w_2}'''' + \frac{\rho A}{EI}\ddot{w_2} + \frac{C}{EI}\dot{w_2} + \frac{K}{EI}w_2 = 0 && x > vt \end{aligned}$$ eq. (4.4)

To obtain the interface conditions we can go to the moving reference frame of the system by means of a variable substitution. This variable change is:

$$\alpha = x - vt$$

After applying coordinate transformation, considering the chain rule in derivation and performing some elaboration (in Annex A), the interface conditions at the position of the load can be formulated and are lined up below. They express the continuity in displacements and slope and illustrate the equilibrium of moment and shear force.

$$\begin{aligned} &w_1(0,t) = w_2(0,t) \\ &{w_1}'(0,t) = {w_2}'(0,t) \\ &{w_1}''(0,t) = {w_2}''(0,t) \\ &{w_1}'''(0,t) = {w_2}'''(0,t) + \frac{P}{EI} \end{aligned}$$ eq. (4.5)

Finally to have a complete description for the problem, we need to specify the boundary conditions. But since the system is infinitely long which implies that no boundary exist, the behavior of the system at infinity (from both sides) can be traced by use of the following relation:

$$\begin{aligned} &\lim_{(x-vt)\to\infty} w_1(x,t) = 0 \\ &\lim_{(x-vt)\to-\infty} w_2(x,t) = 0 \end{aligned}$$ eq. (4.6)

This relation holds in that the bigger the distance becomes from the load, the lower the motion the system experiences. And since the system contains damping, the motion will be absolutely zero.

4.1.2. Steady state solution

The system components, the load, the beam and the foundation are assumed to be in the linear regime. And bearing in mind the fact that the foundation is homogeneous, the response of the system can be expressed as a superposition of harmonic waves. On that basis, the steady state solution will have the following form:

$$w_1(x,t) = \sum A e^{i(\omega t - \gamma x)}$$
$$w_2(x,t) = \sum B e^{i(\omega t - \gamma x)}$$

eq. (4.7)

whereas A and B denote the amplitudes of the harmonic waves, ω the frequency and ɣ the wavenumber. Once these forms have been substituted in the equations of motion in eq. (4.6), the following equation comes out:

$$(\gamma^4 - \frac{\rho A}{EI}\omega^2 + \frac{C}{EI}\omega i + \frac{K}{EI})e^{i(\omega t - \gamma x)} = 0$$

eq. (4.8)

Since the equation needs to be satisfied for all time moments and for all locations, the exponential term can be cancelled out. Basically, the exponent cannot be always zero over time and space. For this reason it may be excluded from the equation while the other expression should be zero. The remaining term will be:

$$\gamma^4 - \frac{\rho A v^2}{EI}\gamma^2 + \frac{Cv}{EI}\gamma i + \frac{K}{EI} = 0$$

eq. (4.9)

The previous expression in eq. (4.9) is called the dispersion equation for free waves. It does not contain any information about the loading term whereas it describes the supporting system. More relevantly, it relates the wavenumber to the frequency. This relation could be further more simplified by means of the so called kinematic invariant equation. The expression can be seen in eq. (4.10)

$$\omega = \gamma v$$

eq. (4.10)

The kinematic invariant relates information about the loading, namely the velocity, to the parameters of the harmonic waves which is then the frequency. It has been previously derived by (Wolfert, 1999) among others. The whole derivation can be found in Annex A. As soon as the kinematic invariant in eq. (4.10) is joined with eq. (4.9), the dispersion equation will read as below:

$$(\gamma^4 - \frac{\rho A v^2}{EI}\gamma^2 + \frac{Cv}{EI}\gamma i + \frac{K}{EI}) = 0$$

eq. (4.11)

The dispersion equation above is a fourth order polynomial which can be numerically solved. The resulting roots represent the wavenumbers and are stated below:

$$\begin{aligned}\gamma_1 &= a + ib \\ \gamma_2 &= -a + ib \\ \gamma_3 &= -a - ib = -\gamma_1 \\ \gamma_4 &= a - ib = -\gamma_2\end{aligned}$$ eq. (4.12)

These roots in eq. (4.12) together with the kinematic invariant expressed in eq. (4.10) are substituted in the solution stated in eq. (4.7). Thereupon, the equations in eq. (4.7) will be rewritten as:

$$\begin{aligned}w_1(x,t) &= A_1 e^{i\gamma_1(x-vt)} + B_1 e^{i\gamma_2(x-vt)} + C_1 e^{i\gamma_3(x-vt)} + D_1 e^{i\gamma_4(x-vt)} \\ w_2(x,t) &= A_2 e^{i\gamma_1(x-vt)} + B_2 e^{i\gamma_2(x-vt)} + C_2 e^{i\gamma_3(x-vt)} + D_2 e^{i\gamma_4(x-vt)}\end{aligned}$$ eq.(4.13)

After the boundary conditions in eq. (4.7) is combined with the general equations in eq. (4.13), the expressions will be reduced to the following:

$$\begin{aligned}w_1(x,t) &= C_1 e^{i\gamma_3(x-vt)} + D_1 e^{i\gamma_4(x-vt)} \\ w_2(x,t) &= A_2 e^{i\gamma_1(x-vt)} + B_2 e^{i\gamma_2(x-vt)}\end{aligned}$$ eq. (4.15)

Now what is only left is to plug the interface conditions and then mathematically, the problem is properly determined.

Once the equations in eq. (4.15) and the interface conditions in eq. (4.5) are merged, the problem is completely solved.

In order to get numerical results, the values used for the different parameters are listed below:

Foundation stiffness	$K = 1.0 \times 10^7$	N/m^2
Foundation damping	$C = 1.0 \times 10^5$	N/m^2
Beam bending stiffness	$EI = 4.89 \times 10^6$	N/m^2
Beam distributed mass	$\rho A = 59.5$	Kg/m
Load amplitude	$P = 14750$	N
Load velocity	$V = 39.0$	m/s

Thereupon, to visualize the behavior of the system, the displacement fields are depicted in the graph below:

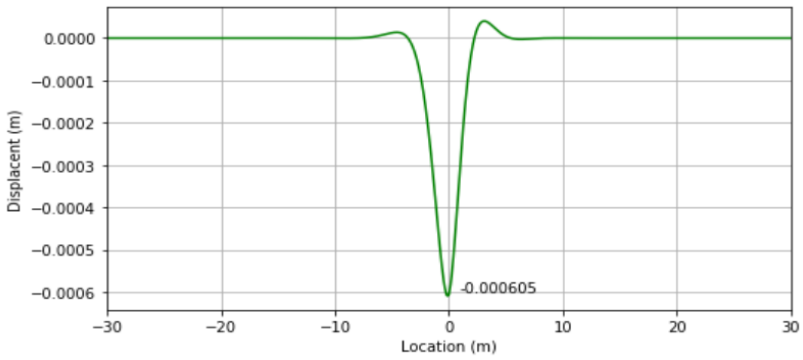

Figure 4.3 Displacement field of a moving load determined analytically

4.2. System including thermal loads

In this section, the considered system is identical to the general system considered in section 4.1. with a single upgrade. As an add-on, axial (compression) loads in the beam are incorporated to account for the rail behavior under temperature.

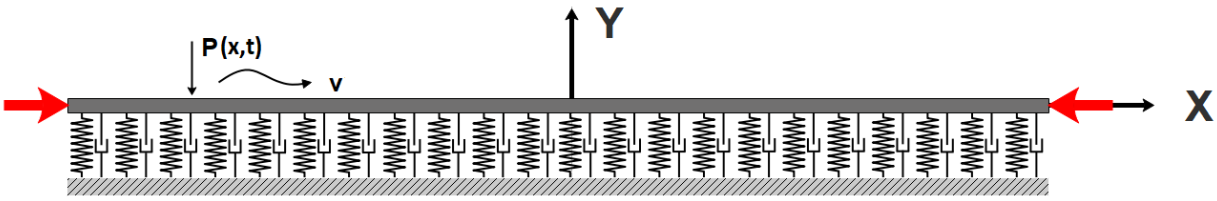

Figure 4.4 Infinite beam on visco-elastic foundation with axial (compression) loads

4.2.1. Mathematical expressions

The governing equations concerning this system are derived in the same form of the general system. The key interventions are highlighted in this sub-section.

The equation of motion in eq. (4.1) gets an additional term as presented by (A.V. Metrikine, 1999) and reads:

$$\rho A\frac{\partial^2 w(x,t)}{\partial t^2}+EI\frac{\partial^4 w(x,t)}{\partial x^4}+T\frac{\partial^2 w(x,t)}{\partial x^2}+C\frac{\partial w(x,t)}{\partial t}+Kw(x,t)=-P\delta(x-vt) \qquad \text{eq. (4.16)}$$

Analogous to the general system, the problem is divided into two domains and approached by the same trial solution like in eq. (4.7). This drives to the dispersion equation stated here:

$$\gamma^4-\frac{(T+\rho Av^2)}{EI}\gamma^2+\frac{Cv}{EI}\gamma i+\frac{K}{EI}=0 \qquad \text{eq. (4.17)}$$

In these equations, T represents the axial (compression) force per unit length of the beam.

$$T = EA \cdot \varepsilon = EA \cdot \alpha_T \cdot \Delta T \qquad \text{eq. (4.18)}$$

whereas EA denote the axial stiffness, α_T the coefficient of thermal expansion and ΔT the change in temperature.

As to the remainder, like discussed before, the roots are obtained, the radiation condition and interface conditions are comprised and lastly the solution is attained.

4.3. Spoormodel validation

In parallel with the analytical approach, the very same problem could be modelled using Spoormodel. For a graphical validation, both displacement fields obtained analytically and by spoormodel are captured together. It is undeniable that both graphs coincide.

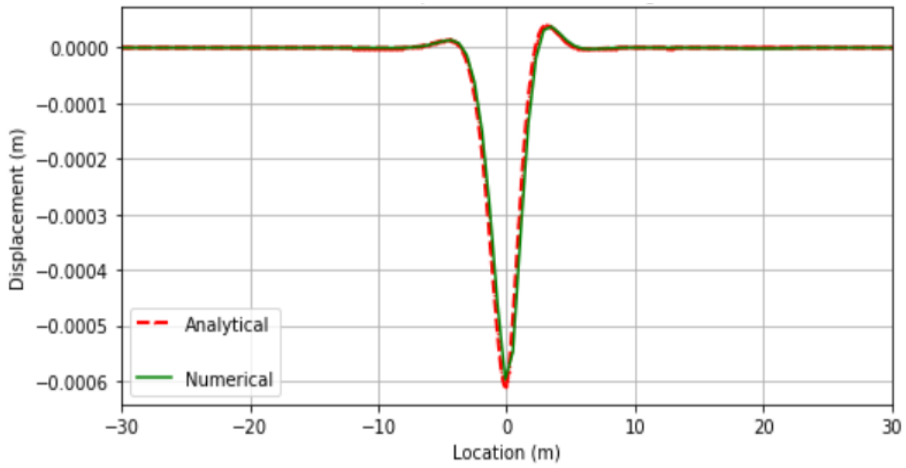

Figure 4.6 Comparing the displacement field from Spoormodel vs the mathematical approach

It is relevant to recall the fact that the validation performed in this sub-section for Spoormodel is just for the steady-state scenario. Nevertheless, this concludes the creditability of Spoormodel.

4.4. GeoVib calibration

After Spoormodel is validated, now time has come to check GeoVib as well. The same problem (which is described below) is modelled by both models to trace any deviations.

The problem includes a train, a track and foundation. The train is composed of a locomotive and three carriages. The track is composed of the 54E1 (UIC54) rails which is widely used in the Netherlands, fasteners and sleepers. The foundation is represented by ground layers whose parameters are given in table 4.5 below (in terms of the cone resistance q_c, the friction f_w, the shear modulus G_{dyn}, the mass density ρ and Poisson's ratio ν).

Carriages	Type	Axle load	Speed
1st, 2nd and 3rd	ICR	10.0 ton	39.0 m/s
4th	TRAXX LOC	23.0 ton	

Table 4.1 Train data

Rail type	Mass	Area	Bending stiffness
54E1 (UIC54)	54.77 kg/m	69.77×10^{-4} m^2	4.89×10^{6} N/m^2

Table 4.2 Rail data

Sleeper type	E-modulus	Mass
Concrete	3.3×10^{10} N/m^2	250 kg

Table 4.3 Sleeper data

Layer depth	Vertical stiffness	Damping
0.5 m	1.5×10^{8} N/m^2	1.0×10^{5} N/m^2

Table 4.4 Ballast data

Type	Depth (m)		q_c (MPa)	f_w (%)	G_{dyn} (MPa)	ρ (kg/m^2)	ν (-)
	from	to					
Sand	0.0	1.5	17	1	149	1700	0.46
Sand	1.5	3.0	20	1	172	1650	0.40
Sand	3.0	10.0	8	1.5	84	2000	0.45
Clay	10.0	11.0	4	2	47	1900	0.48
Sand	11.0	12.0	20	1	172	2000	0.45
Clay	12.0	13.0	2	6	42	1900	0.48
C-S	13.0	14.0	5	2	61	1950	0.47
Clay	14.0	18.0	4	2	49	1900	0.48
Sand	18.0	20.0	20	1	172	2000	0.45

Table 4.5 Foundation data

The trains, rails, sleepers and ballast properties are specified in both models as given in the tables. The foundation data in table 4.5 is specified for GeoVib and translated to a vertical stiffness of (1.0×10^{8} N/m^2) and a damping of (6.5×10^{5} N/m^2) for spoormodel.

Plotting both displacement fields at the rail level together provides a more pronounced picture about how close the results are from the two models to one another. The results are included in the figure beneath:

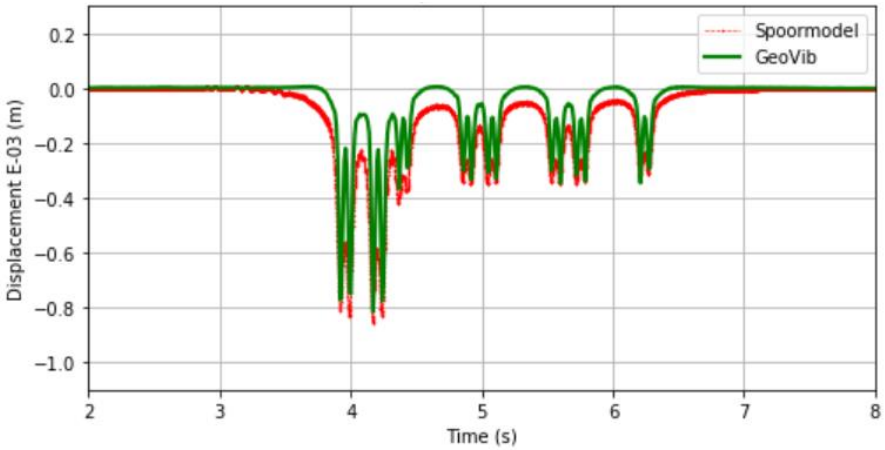

Figure 4.9 Displacement fields at the rail level from Spoormodel vs GeoVib

5. Measurements & data

This chapter contains measurements of the environmental vibrations detected in the vicinity of multiple level crossings in the Netherlands. With a special courtesy from ProRail, this data could be included as to give the reader more evident insight about the problem statement and provide a clear picture of the research targets.

5.1. How it began

Since 2017, ProRail has received a striking number of reports about the increased nuisance caused by vibrations in multiple towns along the railway lines. Not only do the inhabitants complain about the noise, but also about the vibrations that leaves everything shaking including the building self. Based upon a request from ProRail, Movares collected an independent research which concluded that a particular type of passenger train causes considerably more vibrations than other trains. This mainly happens when passing level crossings where differences in the ground (stiffness) create an extra unevenness. In view of these circumstances, ProRail and NS together with the Ministry of I&W started to think about new measures to eliminate the problem and combat the vibration nuisance.

5.2. Mitigation measures

Shortly after that, the ShimLift (previously introduced in section 1.1.) was considered as one of the first measures to counteract vibrations. In 2018, the first tests were performed on the ShimLift as it was applied to one location. The measurements showed a considerable reduction in vibrations. After this first positive result, it was decided to extend the test of the ShimLift to other locations. In 2019, the tests were extended and it was agreed that the ShimLift will remain in place, should the tests yield sufficient results. Unfortunately, months later, the results were found insufficient and that is why other alternatives became a priority.

Furthermore, ProRail is investigating the suitability/feasibility and applicability of three other measures. The first one is a type of foam to be sprayed between the track stones. According to the producer, the soil stress under the stones would be significantly lower owing to the better load distribution in foamed stones. The second proposal is to replace the concrete slab foundation of the level crossing by solid rubber plates. The last one is a kind of cushions to be attached under the sleeper which according to the manufacturer supposed to reduce the vibrations.

On top of that, ProRail, NS and the Ministry of I&W are considering the possibility of lowering the train operational speed on a single route as a test measure. The data and statistics suggested that 10,000 travelers use trains on this route every day. Nevertheless, theoretical calculations showed that the time schedule will accommodate this alteration. In the light of this estimation, it was agreed to drop the speed of the intercity train from 130 to 115 km/h as a test proceeding. This process will last three months. After that, the measurements must show how sufficient this measure is working.

5.3. Measuring process

In order for the assessment of these measures, measurement devices are placed in the vicinity of the track. At one of the houses nearby the level crossing, vibration detectors, image and video recorders are successfully installed under the supervision of Movares. Image and video recorders are included for the possibility to display the (train) load movement and relate that to the resulting vibrations.

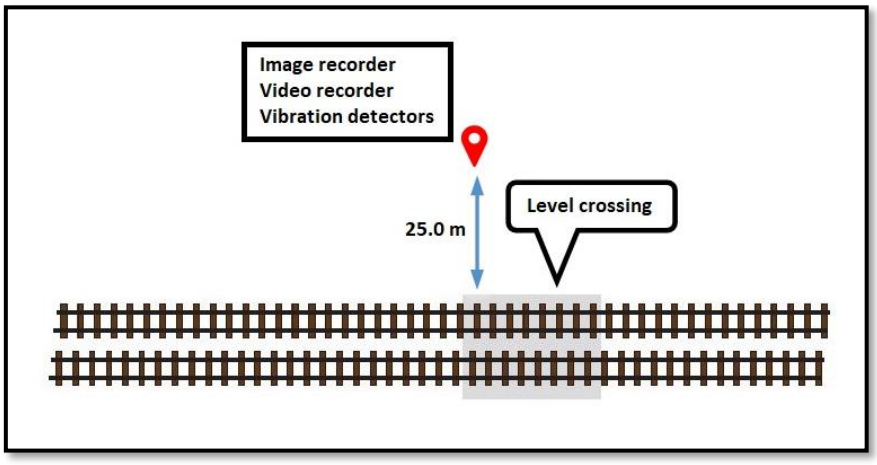

Figure 5.1 Measurement devices located next to the track

Since February 2019, the response is recorded over time. Data is stored, processed and reported continuously.

Figure 5.2 Movares employees install the measurement devices

Figure 5.3 Camera for image and video recording

The team at Movares frequently check the devices and make sure that everything works properly. They also take care of any maintenance needed and assure the success and continuity of the process.

5.4. Data

A part of the registered measurements is presented in this section. Data belonging to two different locations (on the same line 8.0 km apart) will be discussed successively. A brief comparison between both locations in presented in the table below:

	The first location	The second location
Foundation	Sand mixed with clay	Mostly sandy (no clay)
Sun/shadow	Slightly less shadow	Slightly more shadow
Green area (absorbs heat)	Less green area	Larger green area
Tracks	Two tracks	Two tracks

Table 5.1 Dissimilarities between the locations

5.4.1. The first location

This first location is the most critical one in terms of vibration intensities and it includes two way tracks. In addition to the vibration results, some more analysis are added like the temperature distribution and the frequency spectrum.

5.4.1.1. Vibrations

A graphical representation of the ground vibration intensities through time can be visualized below in Figure 5.4. A brief overview of the results is included.

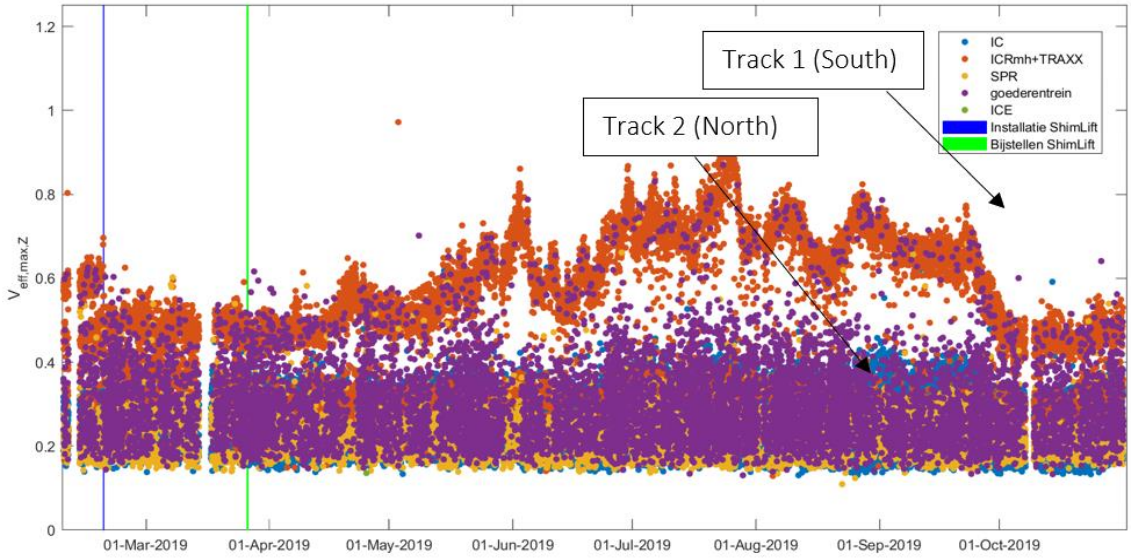

Figure 5.4 Vibrations vs time for location 1

As previewed in the figure, the resulting vibrations due to the different types of trains are distinguished clearly. The freight train vibrations are marked in purple, the Sprinter (SPR) vibrations in yellow, the Intercity Express (ICE) vibrations in green, the regular Intercity (IC) vibrations in blue and lastly the combination of the Intercity with TRAXX locomotives (ICRmh+TRAXX) vibrations in red.

As mentioned earlier and highlighted in Figure 5.4 above, the vibrations caused by a particular train type (being the combination of the Intercity with TRAXX locomotives (ICRmh+TRAXX)) are significantly higher than those caused by the rest. There is a major difference between the two tracks as the southern track gives considerably higher values. This could be a consequence of alignment issues or due to some more irregularities.

It is worth noting as well that the ShimLift was installed in February and became in action ever since. That is highlighted in the figure by means of a vertical blue line on the left side of the graph. After nearly a month, the ShimLift was adjusted as a matter of maintenance. That is also highlighted in the figure by a green line shortly after the blue one in the timeline.

As a result of the ShimLift installation, the leading/maximum vibrations dropped immediately about 30%. After about three weeks from the adjustment of the ShimLift, the vibrations on the southern track increased again to the original value and consequently slightly reduced.

Following that, and after some fluctuations, it started rising gradually until reaching the absolute maximum at the end of July. Afterwards, it started declining progressively until reaching values comparable to those at the very beginning.

To sum up, it should be recalled that the leading vibrations are mostly resulting from the combination of the Intercity with TRAXX locomotives (ICRmh+TRAXX), although freight trains occasionally cause similar magnitudes. Another interesting part is the southern track giving higher values. And finally, the peak period takes place between May and October.

5.4.1.2. Temperature distribution

Based on the conclusions drawn on the vibration results in Figure 5.4 especially the peak values being in the summer months, it became consistent to contemplate the climate conditions and temperature and how it relates to the vibrations.

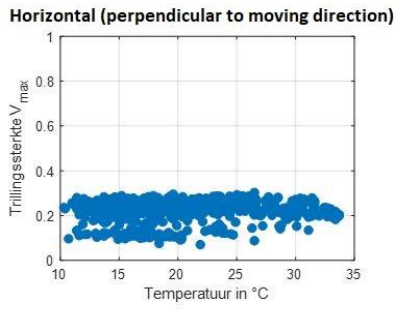

Figure 5.5 Horizontal vibrations vs temperature

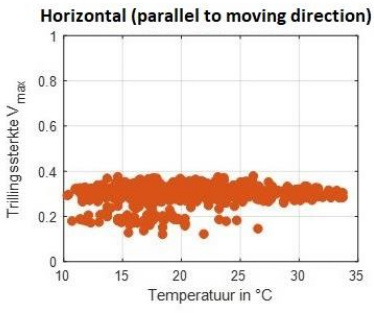

Figure 5.6 Horizontal vibrations vs temperature

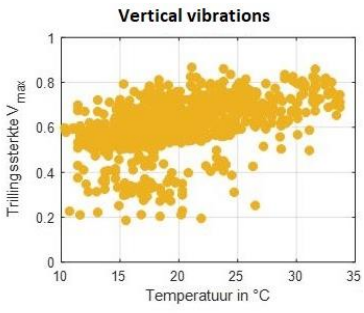

Figure 5.7 Vertical vibrations vs temperature

The relation between the temperature and the vibrations is demonstrated in the figures above. The figures indicate that the horizontal vibrations are not highly influenced by the temperature. By contrast, the right side figure shows that the vertical vibrations are to some extent dependent on the temperature.

5.4.2. The second location

This second location has lower values than the first location in terms of vibration intensities. Besides, it follows to some extent a different pattern through time.

5.4.2.1. Vibrations

A graphical representation of the ground vibration intensities through time is shown below in Figure 5.11. A brief overview of the results is included.

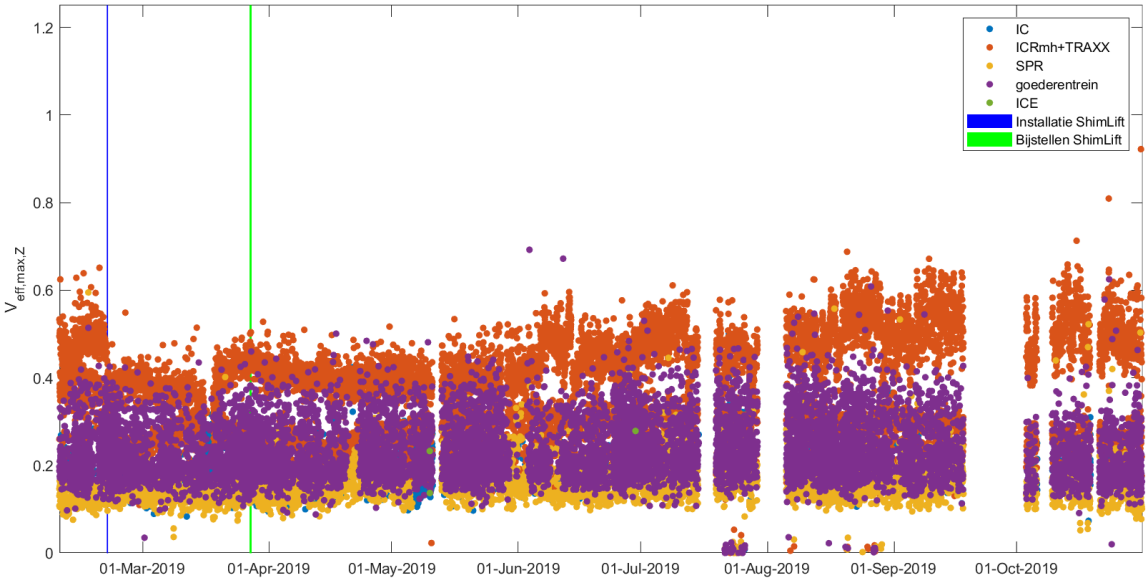

Figure 5.11 Vibrations vs time for location 2

As presented in the figure, and similar to the situation in location 1 the resulting vibrations due to the different types of trains are distinguished clearly. The freight train vibrations are marked in purple, the Sprinter (SPR) vibrations in yellow, the Intercity Express (ICE) vibrations in green, the regular Intercity (IC) vibrations in blue and lastly the combination of the Intercity with TRAXX locomotives (ICRmh+TRAXX) vibrations in red.

Likewise, in corresponding with location 1, the vibrations caused by a particular train type (being the combination of the Intercity with TRAXX locomotives (ICRmh+TRAXX)) are considerably higher than those caused by the rest. But on the other hand, the difference between the two tracks is quite limited and not as high as in the first location. A potential reason for these dissimilarities could be that the two tracks in the first location are not as close to each other as in the second location.

Following the process of ShimLift installation (highlighted in the figure by a vertical blue line on the left side), the leading/maximum vibrations dropped immediately about more than 30%. After that and along roughly three weeks the vibration level remained fairly stable before it started again increasing. Since the adjustment of the ShimLift (highlighted in the figure by a vertical green line on the left side), the governing vibrations dropped gradually and maintained a stable level until mid-May.

Moving on from mid-May the vibration level grows in a gradual manner until October and then it tends to withdraw. It should just be underlined here that this growing attitude is not completely continuous, as the it undergoes some fluctuations and wobbles. Among a few, there is an obvious fall out during the last third of July with a turnaround in the first week of August.

In opposition with the first location, some of the variations that occur here cannot be correlated with the ambient temperature. While some of the peaks in the first location existed during hot periods, the same cannot be stated here. Another key difference is the maximum vibration intensity which does not match in both locations. The first location recorded the highest values as the second location reached only 65% of the peak value at location 1. And lastly, the decisive vibrations in the first location were almost always related to the combination of the Intercity with TRAXX locomotives (ICRmh+TRAXX) with the freight trains occasionally strike similar values. This statement does not comply with the situation here as only fewer freight trains during a certain period of the timeline could be noticed.

In the figure throughout the timeline, there are some gaps mainly in July, August and September. During these periods the measuring system had issues and therefore no data have been recorded. Accordingly, the hardware has been upgraded and so the malfunctions were adjusted.

To sum up, in this situation the leading vibrations are almost purely resulting from the combination of the Intercity with TRAXX locomotives (ICRmh+TRAXX). There are some fluctuations that could be spotted throughout the timeline but no real peak was observed.

5.4.3. General conclusions about the measurements

Based upon the previously previewed data and measurements, the following conclusions were made:

- Regarding the ShimLift as a mitigation measure, it could be deduced that it has impact, but not always noticeable (about 30% effect). With time, its impact in some locations diminishes, and therefore maintenance and adjustment are frequently implemented.
  After the adjustment, the effect is not always and everywhere the same, meaning that there are situations when we get positive results, negative results or no difference at all.
  It is even more striking that the ShimLift in some situations seem to be counterproductive and vibration level grows as a consequence. This could be due to the fact that some locations were already flat before the ShimLift installation.
  It is quite obvious that the ShimLift has a major influence on trains with higher vibrations like the combination of the Intercity with TRAXX locomotives (ICRmh+TRAXX), while the other train types being barely effected. This could be related to some differences in properties between these train types like the unsprung mass.
  Ultimately, the ShimLift is applied manually and this could be an explanation for any illogical results. The level of accuracy is also decisive and need to be taken into consideration. This is one of the aspects about the ShimLift that could be further improved.

- The combination of the Intercity with TRAXX locomotives (ICRmh+TRAXX) gave higher vibrations in some of the locations in April, while in other locations between May and August. These months are all in the summer period and that is why a relationship between the ambient temperature and vibration level could exist.

- For some different locations the results were not identical or even comparable. In such situations it is reasonable to consider the variances in foundations and soil layers. Even for the same location, there are situations when two tracks give significantly higher or lower results. This could be related to the track alignment or due to some more irregularities.

- At different time moments during the same season and occasionally at the same location different results were experienced. Fact of the matter is that the number of passing trains is not always identical.

6. Results and discussion

In this chapter, a full analysis is performed using the previously presented (GeoVib and Spoor-) models in order to investigate the effects of the three scenarios: foundation inhomogeneity, the hanging sleepers and the temperature.

The global model which is used in this parametric study consists mainly of a train, a track and foundation. The train includes a locomotive and three carriages. The track is composed of the 54E1 (UIC54) rails, fasteners and sleepers. The foundation is comprised of the ground layers at one of the locations addressed in this project. The model is well described with the specified parameters in section 4.4.

6.1. Transitions

As already prescribed in the introduction, railways are not continuously uniform along the whole track. There are transitions and shifts, that the track undergo. These changeovers could have an influence on the track performance and the response to the loads. A small analysis will be performed in order to investigate these consequences.

6.1.1. Foundation inhomogeneity

In this scenario, we investigate the influence of the level crossing. To do this, the track changes from a ballasted track to a slab track and then back to a ballasted track. In this context, there is a consecutive stiffness change in the track which is more likely to have an impact on the track response to the loads. This will be investigated in this section.

A model with a uniform track (Figure 6.1) is compared to the same model with a track containing the level crossing (Figure 6.2). The observed results are included below:

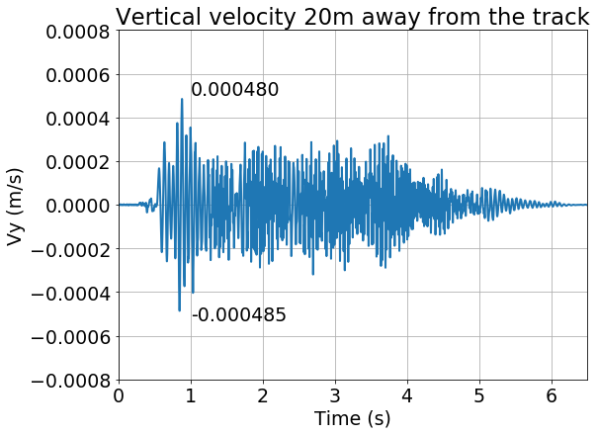

Figure 6.1 Response vibrations (Neutral model)

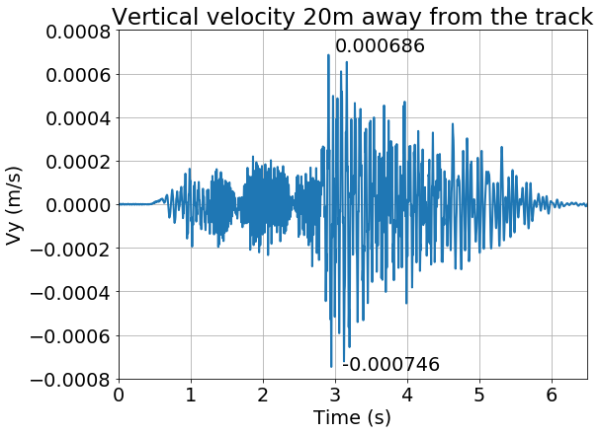

Figure 6.2 Response vibrations (with a level crossing as a foundation inhomogeneity)

The graphs validate the statement that the existence of a level crossing along the track affects the response whose maximum is namely increased by about 42%. Nevertheless, we can see that the maximum in the neutral model is at nearly 1 sec while in the nonhomogeneous stiffness model it is at 3 sec. This can be due to the fact that the train is approaching the level crossing which is located exactly in the halfway of the track distance. It is also obvious that there is one maximum in the neutral model. This happened because the locomotive is heavier and leads to a larger response. The amount of noise in the graphs can be related to the timestep in the model and it can be improved by defining a smaller timestep. Although this is the case, we expect that the results will not considerably change for decreasing it.

6.1.2. Hanging sleepers

One of the relevant cases in this project is the early mentioned hanging sleeper scenario known as the blinde-vering. Being encountered multiple times at different locations in the field as stated in the previous chapter, it became significant to analyze it and study the effects.

The hanging sleeper scenario was represented by the nonlinear behavior of the springs previewed in Figure 6.3. For upward displacement of the rail, the spring does not possess any stiffness as the soil is not expected to react to tension forces. For downward displacement of the rail, we have a suspended connection of 2mm beyond which the spring is in action again with the standard stiffness.

Figure 6.3 Stiffness of elements in the hanging sleeper area

The analyzed scenario includes a ballasted track without hanging sleepers (in other words, continuous contact between rail and supporting track) going to a portion of 4.5 m of the track in which hanging sleepers are implemented, after which the rail is again in continuous contact with the supporting structure. This is implemented in Spoormodel, while for GeoVib the effect of the hanging sleepers is incorporated just in the load from the vehicle. And for clarity, it must be noted that the model is symmetric, as the domains before and after the hanging sleeper portion are the same as long.

A distinction between the response of a standard connected foundation element and a foundation element in the hanging sleeper domain is depicted in Figure 6.4 below. Besides the huge difference spotted in the displacement under the load (nearly 4 times higher), a slight deviation can be recognized in the absence of the load as well. This reflects upon the fact that the track in this instance bends under its own weight.

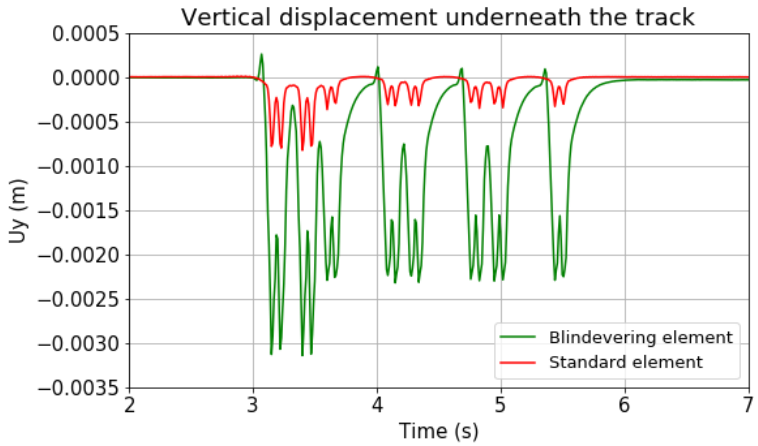

Figure 6.4 Hanging sleeper effect plotted by Spoormodel

The graphical representations below offer a visualization of how sensitive the track can be to the hanging sleepers situation. In terms of the response, we face a huge enlargement in the maxima (more than 10 times higher), but also a noticeable difference in the amount of noise in the results. This indicates how significant the dynamic effect is in the model with hanging sleepers. Furthermore, the extremes in both figures are not at the same location because the hanging sleeper domain is in the middle of the track distance. Finally, it should be highlighted here that the vibrations recorded during the first second of time in Figure 6.6 can be related to the initial conditions and therefore maybe neglected.

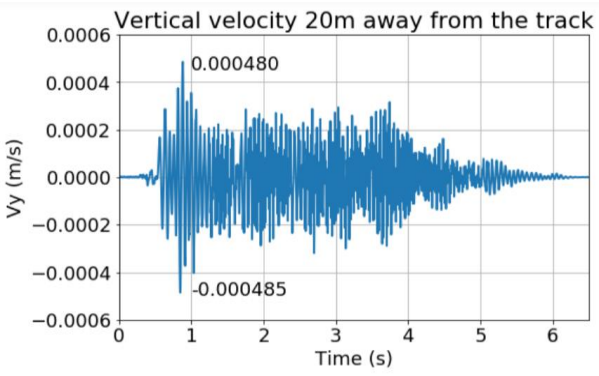

Figure 6.5 Response vibrations (Neutral model)

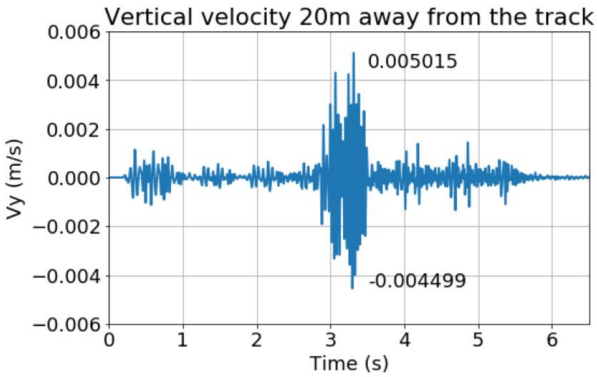

Figure 6.6 Response vibrations (with hanging sleepers)

6.2. Temperature

Nowadays, the rails are continuously welded. This is motivated by many reasons like the reduced energy and maintenance costs, the less noise and vibrations and the more ride comfort. On the other hand, this could be a disfavor in other aspects like the thermal behavior, where no room is left for thermal expansion. This can lead to high compressive stresses and maybe heat distortions. With regard to that, some instances are analyzed in this section.

6.2.1. Axial stresses

In hot periods, particularly during the summer, forces pile up in the rail which entails high axial stresses. These stresses can impact the behavior of the rails which urges against omitting them in the design.

In this context, to determine the effect of axial stresses, a thermal expansion coefficient of (12E-06) and a temperature difference of 55°c were specified for the rails. This gave rise to an axial (compression) force in the rails. Afterwards, the response was then identified and plotted against neutral model. The results are presented here:

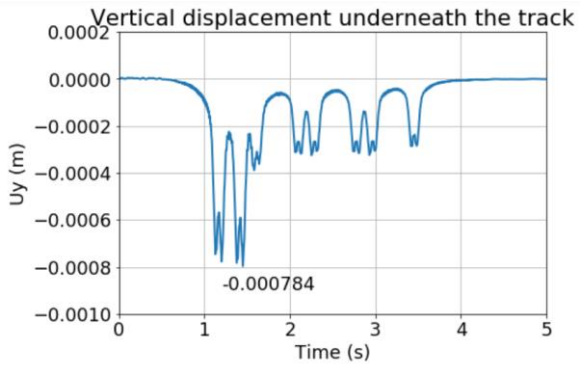

Figure 6.7 Response vibrations (Neutral model)

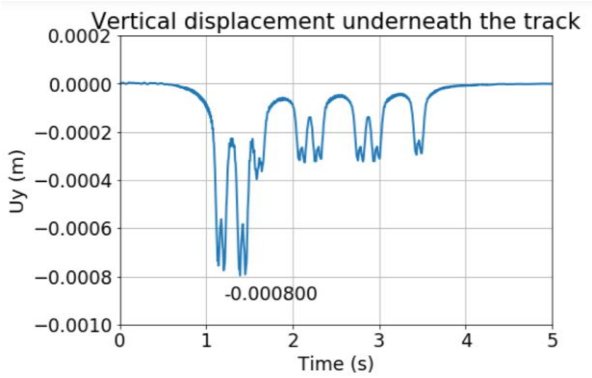

Figure 6.8 Response vibrations (with a thermal load)

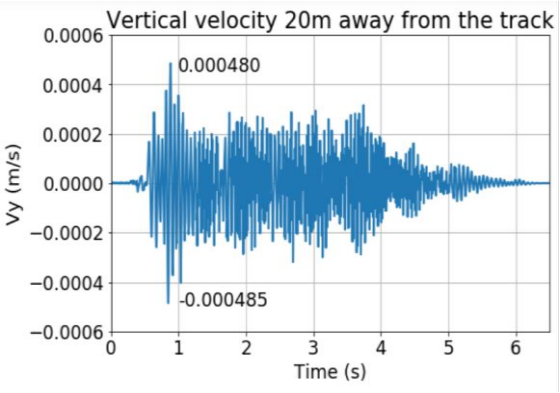

Figure 6.9 Response vibrations (Neutral model)

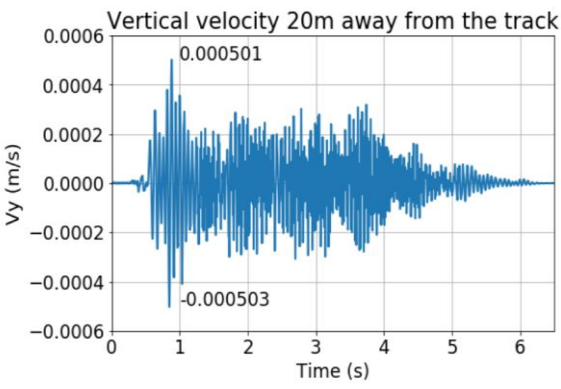

Figure 6.10 Response vibrations (with a thermal load)

The upper pictures display the near field response expressed in displacements which is recorded under the track at the sleepers. The latter pictures reveal the far domain response illustrated in the form of velocity vibrations and measured at a distance of 20 meters away from the track.

The figures have demonstrated the influence of the thermal loads. Inasmuch as the vibrations have the same course, the model with thermal expansion shows a higher response. While the velocity vibrations peak exhibit a difference of nearly 4.5%, the displacement fields appear to shift with slightly less percentage. The graphs show also that both peaks are at the same time around 1 sec. Finally, the amount of noise in both graphs is similar and is related to the timestep in the model.

The analytical approach showed consistency with these results. An axial force of (970.2 KN/m) was incorporated in the rail beam, which is the resultant force due to the thermal expansion. This was computed on the basis of the previously mentioned values of the expansion coefficient, the Young's modulus and cross-sectional area of the rail beam. It appeared also from spoormodel that rail was prone to a matching level of axial load. The results indicate that the displacement field increased by about 4%.

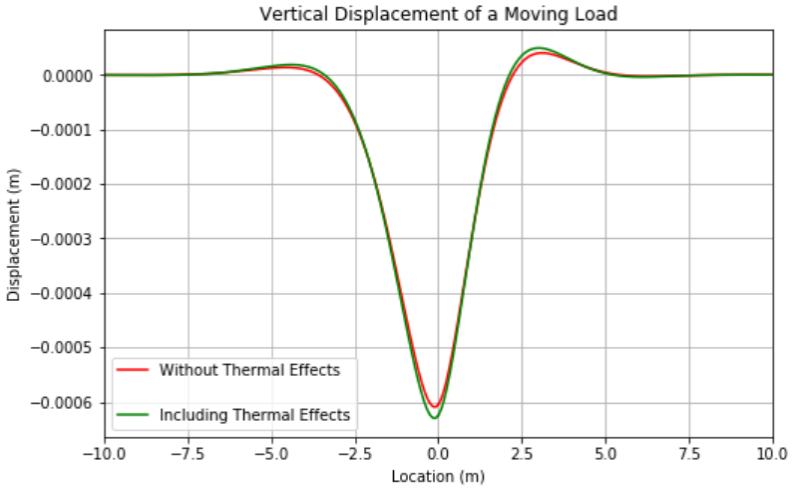

Figure 6.11 The thermal expansion effect assessed analytically

6.2.2. Changing properties due to changing temperature

Owing to sun heat and the elevated ambient temperature in warm periods, the rail absorbs the heat and becomes far hotter. That increased temperature does not leave the performance in place. The properties of rails and the rail pads will be affected as well. The thermal dependence of the viscoelastic rail pads was illustrated earlier in chapter two. The shear modulus, stiffness and damping all have a strong correlation with the temperature. All these characteristics experience a negative impact with the temperature. Alongside that, the stiffness of rails can suffer some minor implications.

In this part, a change in the track properties was considered. The rail pad stiffness was lowered by 30%, the rail pad damping by 15%, the shear modulus by 10% and the rail stiffness by 10%. It must be noted that these alterations can be referred to the literature namely in the sections following-up to 2.4. (where thermal effects are addressed), bar the last one regarding the rail stiffness. The reduction in the rail stiffness due to increased temperature is a rough estimation and is not found in the literature. Although this reduction may be on the high end, it merely shows what can be expected in extreme situations. After applying these modifications, the response was compared to the neutral model. The results are shown here:

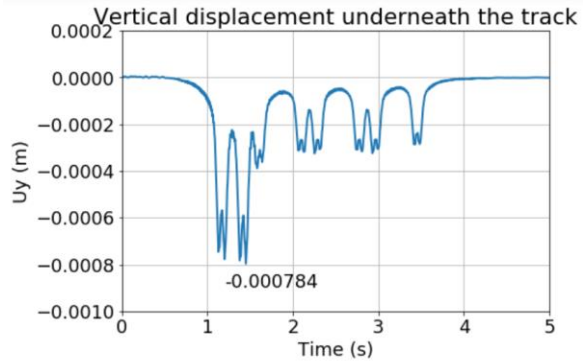

Figure 6.12 Response vibrations (Neutral model)

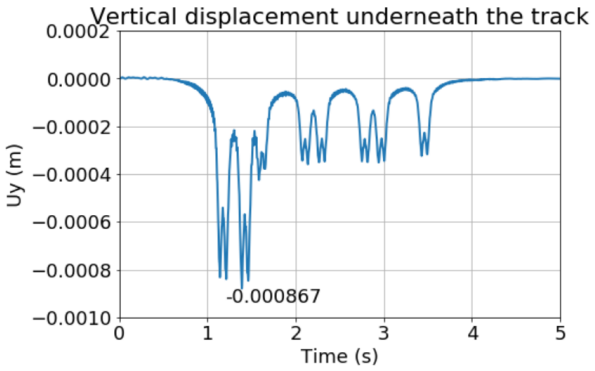

Figure 6.13 Response vibrations (reduced properties)

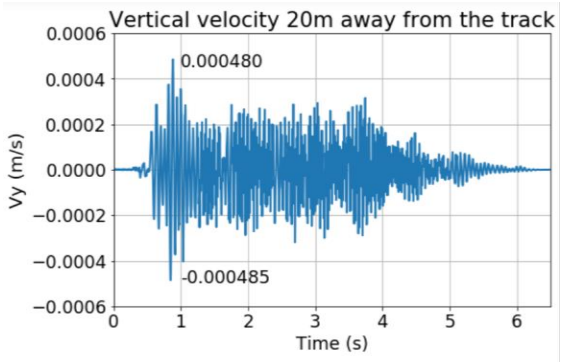

Figure 6.14 Response vibrations (Neutral model)

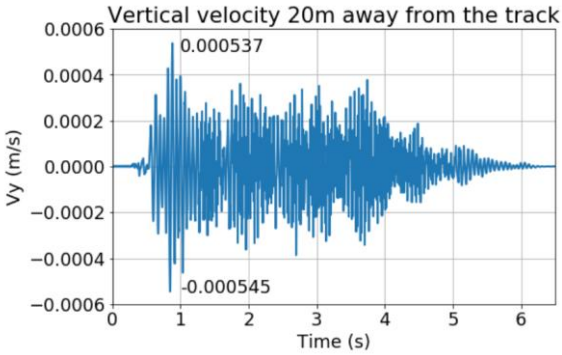

Figure 6.15 Response vibrations (reduced properties)

As one would predict, the displacement fields under the track as well as the velocity vibrations 20 meters away illustrate a difference in the magnitudes. The figures reported a rise of 10.5% in the displacement maxima's and even more than 12% in case of the velocity. Following these thermal-related drops in the track properties, is was not far beyond the expectations that the vibration level will get amplified. The noise level is again similar in both graphs and is related to the timestep in the model.

According to section 2.2.2, the velocity vibrations were expected to drop to some extent as a consequence of lowering the track stiffness. Nevertheless, this is not what we found here when the track stiffness was reduced as explained before. The reason behind this could be the fact that changing the other properties like rail pad stiffness and damping along with the shear modulus has a stronger impact than reducing the track stiffness.

Complementarily and as a check process, the same evaluation is performed using the analytical approach (section 4.1.). Nevertheless, not much of a discrepancy with the numerical results was found. Analytically, the obtained results were in line with the numerical ones. It was found that by modifying the track properties as specified above, the response gets enlarged by about 13%.

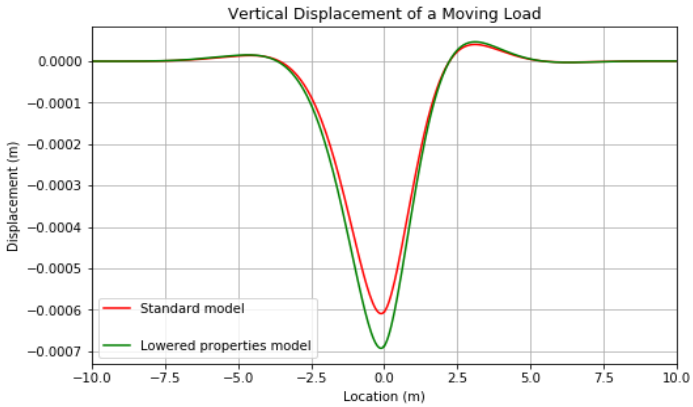

Figure 6.16 The effect of reducing model mechanical properties assessed analytically

After both numerical and analytical results being similar, it is quite relevant to highlight that the simple analytical approach was sufficient enough to review this effect.

6.2.3. Track irregularity due to temperature increase

Numerous train vehicles passing over the track create vertical uplift and hunting motion which reduce the resistance of the track. And following the high compressive forces caused by thermal and mechanical sources, while no expansion possible, the rail could tend to undergo deformations as highlighted in the upcoming figures. In extreme cases even heat distortion is likely to happen.

Figure 6.17 Rail deformation vertically (heat_distortion, 2009)

Figure 6.18 Rail deformation laterally (NetworkRail_news, 2019)

As the track resistance withdraws, the rails get more flexibility to deform under axial loads. As the figures show, deformation could take place either laterally or vertically.

In view of this, the thermal effect was included in an indirect approach by imposing an irregularity to the rail as a result of deformation. This model can be found in Annex A.

6.3. Thermal loads with hanging sleepers

After the effect of the hanging sleeper and thermal expansion is checked independently each, now both are considered in the same simulation to track the group impact.

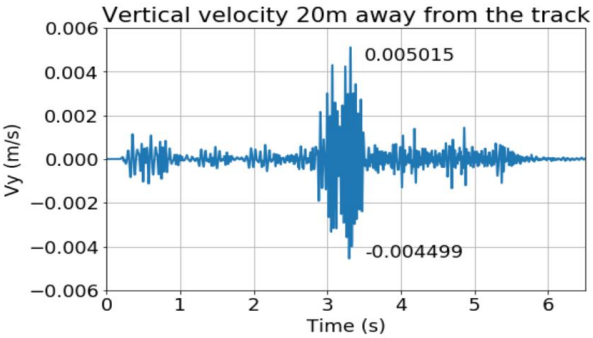

Figure 6.19 Response vibrations (with hanging sleepers)

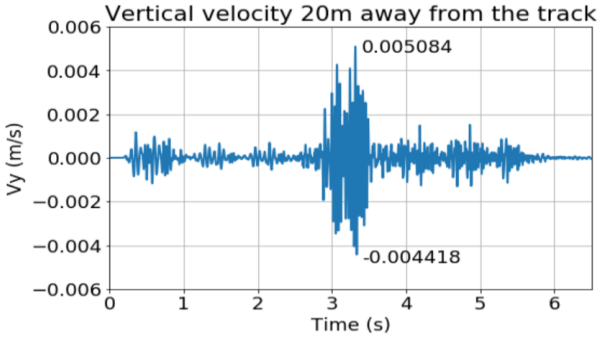

Figure 6.20 Response vibrations (thermal + hanging sleepers)

The results present a clear difference with the neutral model as well as the model with thermal expansion only in Figures 6.9 and 6.10 respectively. Particularly more important, the vibrations peak here is also just higher than in the model with hanging sleepers. In the wake of the huge hanging sleepers impact, the group impact does not seem to be striking. The vibrations measured during the first second of time in both figures are related to the initial conditions and therefore maybe neglected. Ultimately, one can conclude that the temperature effect is hardly noted in the presence of hanging sleepers scenario.

6.4. Thermal loads with a foundation inhomogeneity

Similar to the previous section, here we simulate the impact of both the thermal expansion and the foundation inhomogeneity in one model, after being both checked independently each.

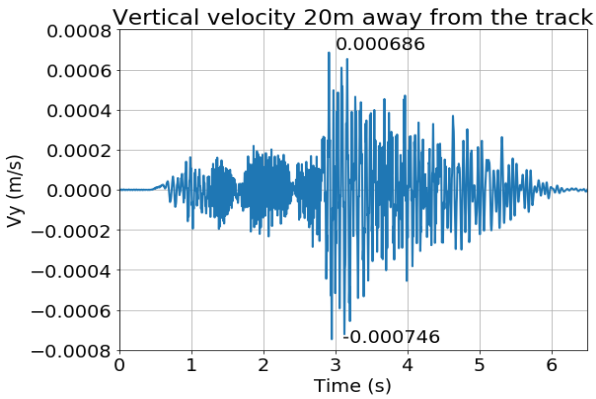

Figure 6.21 Response vibrations (with foundation inhomogeneity)

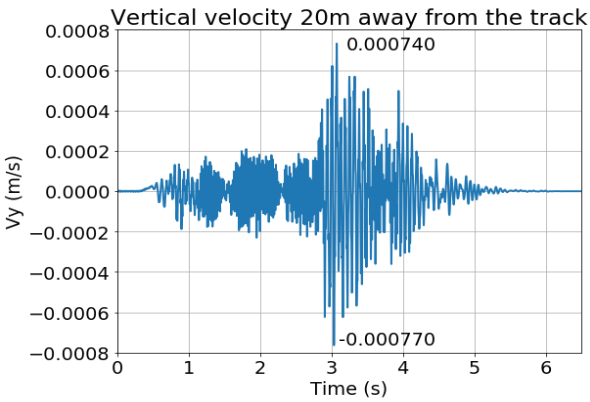

Figure 6.22 Response vibrations (thermal + foundation inhomogeneity)

Similar to the previous section, the results present a clear difference with the neutral model as well as the model with thermal expansion only in Figures 6.9 and 6.10 respectively. In addition to that, the vibrations peaks here are also higher than in the model with a nonhomogeneous foundation. In section 6.1.1. namely where the impact of the foundation inhomogeneity was examined, a deviation of 42% in the results was noted. In this case after assessing the group impact it is found raised up to 59%. Here it turns out that the thermal expansion effect is more momentous than in the scenario of hanging sleepers and thermal effects.

6.5. Combination of all of the above

Finally to get a grip on the complete picture, all these factors (hanging sleepers scenario, temperature and the foundation inhomogeneity) are assembled here to study the group impact.

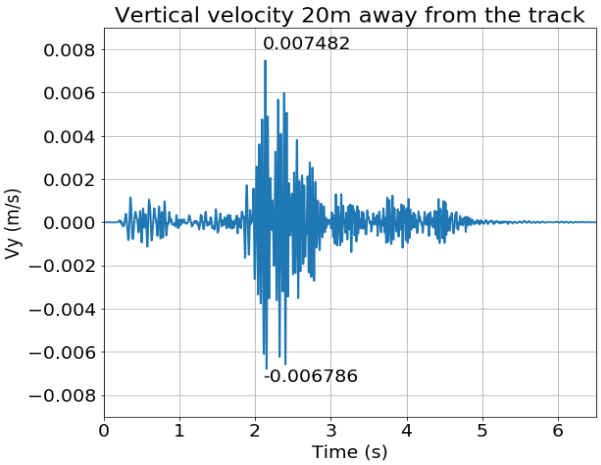

Figure 6.23 Response vibrations (with foundation inhomogeneity + hanging sleepers)

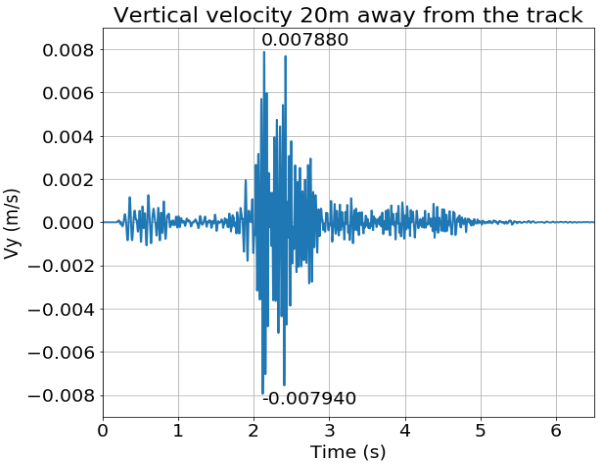

Figure 6.24 Response vibrations (foundation inhomogeneity + hanging sleepers + thermal load)

After investigating the effects of these factors individually and reviewing them one by one, it is relevant to simulate them concurrently analyze the response.

The results show a clear difference with the model without thermal loads on the left side, with peak vibration difference of nearly 5.5%. Furthermore, the graph on the right side which included all the three factors, recorded higher values than the separate cases of these factors (see the previous sections). It should be recalled again here that the vibrations measured during the first second of time in both figures can be neglected because they are related to the initial conditions.

The graphs have illustrated a substantial influence which is more certainly higher than in any of other cases. This provides an enlightenment of what we can expect if all these factors get involved in the problem.

7. Conclusions and Recommendations

At long last, and after finalizing this parametric study, this research is coming to a close. Ultimately, the main outcomes will be emphasized and essential actions will be recommended in the light of the foregoing finding.

7.1. Conclusions

The objective of this thesis was to determine the influential parameters in terms of the response vibrations in the proximity of railway tracks. In such a way it was suggested following the theoretical study and in view of the measured data to investigate a set of three factors (being the ambient temperature effect, the hanging sleeper scenario and the inhomogeneity of foundation) and analyze their impacts.

1) The inhomogeneity of the foundation possesses a significant influence on the vibrations in terms of amplitudes as well as the level of noise and signal interference. It was found that the existence of a level crossing along the track affects the response whose maximum is increased by nearly 42%.
2) The hanging sleeper scenario has a momentous effect not only in terms of the response vibrations which get massively amplified but also troublesome regarding the operation process. Accordingly, the maximum displacement increased nearly 4 times, while velocity vibrations got enlarged and the peak namely increased more than 10 times. Over and above, the high dynamic effect highlighted in the results could lead to quality deterioration and even worse to destabilization and derailment in extreme cases.
3) The ambient temperature in normal conditions holds a minor effect that could be drastic in severe conditions. It was found through direct thermal models (in section 6.2.1.) that the response peak increases by 4.5%. The indirect thermal models (in section 6.2.2. and 6.2.3.) present higher amplifications up to 12%. Furthermore, it was found through calculations that the higher the axial force in the rails become, the more the vibrations will get amplified. This emphasizes how hefty the consequences may become.

It must be recalled here that the data analysis of the measurements underlined considerable enlargements in the vibrations during hot periods and the summer season. On these grounds the following questions popped up upon advancing through the results of the current research.

1) What are the chances that the ShimLift can gets impacted by the ambient temperature and in this instance how vigorous would this effect be?
2) In what sense does the rail experience deformations due the ambient temperature and following any thermal expansion? And can the rail alignment be affected as a result?

7.2. Recommendations

In this section, in the wake of this research some recommendations will be discussed.

- As mentioned in the previous section, the temperature could have an effect on the performance of ShimLift. Therefore, it would then be appropriate for the temperature dependence of the ShimLift should be investigated.
- In the present dissertation the hanging sleepers effect was studied. Nevertheless, due to time limitations the phenomenon was not scrutinized in a broad prospect manner. Accordingly, it is urged to conduct follow-up investigations, regarding the mechanism in the following instances:
  - When the phenomenon gets activated in smaller domains or just couple of sleepers.
  - When the phenomenon gets activated in larger domains.
  - When the phenomenon is in action at more locations in the same neighborhood or on the same track.
- It was illustrated during this research that the axial loads in the rails when they exceed a certain limit, the response then blows up. So a further research topic would be to check in so insofar as possible what could lead the axial loads in the rails (due to thermal effects or else) to increase.
- Another related question would be about the possibility whether the rails could get over-warmed such that it becomes sometimes unstable?
- Furthermore, it is advisable to keep the rail alignment frequently in check to be alert on any hanging sleepers situations and to be aware of any rail deformations.

Annex A

❖ Deriving the system's equation of motion

In this section the equation of motion for the considered system is derived and discussed as referred in section 4.1.1. The system is displaced upwards and the acting forces are presented in the picture below:

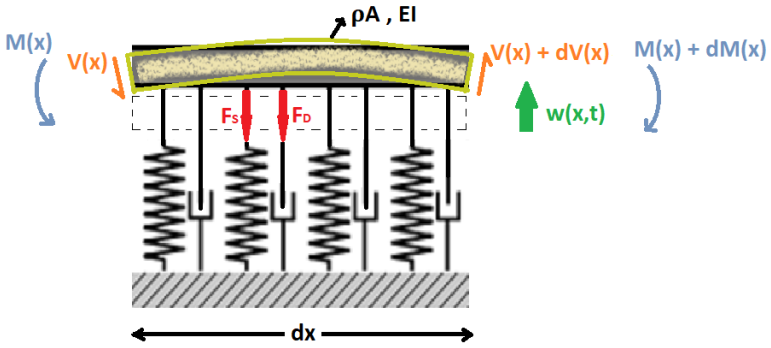

Figure A.1 Force diagram (of an infinitesimal element)

If we consider the balance of moments, the following condition is obtained:

$$V(x) = \frac{\mathrm{d}M(x)}{\mathrm{d}x} \qquad \text{eq. (A.1)}$$

Consequently, to derive the equation of motion, we consider the equilibrium of vertical forces in the force diagram above.

$$\rho A \cdot dx \cdot \frac{\partial \dot{w}}{\partial x} = \sum forces \qquad \text{eq. (A.2)}$$

The acting forces are included, being the spring force, dashpot force and the shear force:

$$\rho A \cdot dx \cdot \frac{\partial \dot{w}}{\partial x} = -F_S - F_D + dV \qquad \text{eq. (A.3)}$$

Now we substitute the forces:

$$\rho A \cdot dx \cdot \frac{\partial \dot{w}}{\partial x} = -K \cdot w \cdot dx - C \cdot \dot{w} \cdot dx + dV \qquad \text{eq. (A.4)}$$

By dividing by dx we get the following expression:

$$\rho A \cdot \frac{\partial \dot{w}}{\partial x} = -K \cdot w - C \cdot \dot{w} + \frac{dV}{dx} \qquad \text{eq. (A.5)}$$

If we involve the condition in eq. (A.1), we get:

$$\rho A \cdot \frac{\partial \dot{w}}{\partial x} = -K \cdot w - C \cdot \dot{w} + \frac{d}{dx}\left(\frac{dM}{dx}\right) \qquad \text{eq. (A.6)}$$

At the same time we bear in mind the following conditions:

$$M = EI \cdot \kappa = EI \cdot \left(\frac{d\varphi}{dx}\right) = EI \cdot \left(\frac{d}{dx}\left(\frac{-dw}{dx}\right)\right) \qquad \text{eq. (A.7)}$$

From the expression in eq. (A.7), we find:

$$M = -EI \cdot \left(\frac{d^2 w}{dx^2}\right) \qquad \text{eq. (A.8)}$$

Since the beam is prismatic, the derivative of the moment becomes then:

$$\frac{dM}{dx} = \frac{d}{dx}\left(-EI \cdot \frac{d^2 w}{dx^2}\right) = -EI \cdot \frac{d^3 w}{dx^3} \qquad \text{eq. (A.9)}$$

By taking again the derivative of the previous equation, it reads:

$$\frac{d}{dx}\left(\frac{dM}{dx}\right) = \frac{d}{dx}\left(-EI \cdot \frac{d^3 w}{dx^3}\right) = -EI \cdot \frac{d^4 w}{dx^4} \qquad \text{eq. (A.10)}$$

Finally, after combining both equations eq. (A.6) and eq. (A.10) we get the equation of motion:

$$\rho A \cdot \frac{\partial^2 w}{\partial t^2} + C \cdot \frac{\partial w}{\partial x} + EI \cdot \frac{\mathrm{d}^4 w}{\mathrm{d}x^4} + K \cdot w = 0 \qquad \text{eq. (A.11)}$$

❖ Coordinate transformation

Furthermore in section 4.1.1, it is stated that the coordinate transformation applied which may imply some changes in the differential equation. This will be addressed here:

$$\alpha = x - vt \qquad \text{eq. (A.12)}$$

Starting from the expression in eq. (A.12), the coordinate switches from x to α, which means the space derivative is no longer dw/dx but becomes $dw/d\alpha$.

And the first time derivative follows:

$$\frac{\mathrm{d}w}{\mathrm{d}t} = \frac{\mathrm{d}w}{\mathrm{d}\alpha} \cdot \frac{\mathrm{d}\alpha}{\mathrm{d}t} + \frac{\mathrm{d}w}{\mathrm{d}t} \cdot \frac{\mathrm{d}t}{\mathrm{d}t} \qquad \text{eq. (A.13)}$$

where $\frac{\mathrm{d}\alpha}{\mathrm{d}t} = -v$ and $\frac{\mathrm{d}t}{\mathrm{d}t} = 1.0$.

Joining these conditions with eq. (A.13), it becomes:

$$\frac{\mathrm{d}w}{\mathrm{d}t} = \frac{\mathrm{d}w}{\mathrm{d}\alpha} \cdot (-v) + \frac{\mathrm{d}w}{\mathrm{d}t} \cdot (1.0) \qquad \text{eq. (A.14)}$$

The second time derivative can then be formalized:

$$\frac{\mathrm{d}^2w}{\mathrm{d}t^2} = \frac{\mathrm{d}}{\mathrm{d}t} \left\{ \frac{\mathrm{d}w}{\mathrm{d}\alpha} \cdot \frac{\mathrm{d}\alpha}{\mathrm{d}t} + \frac{\mathrm{d}w}{\mathrm{d}t} \cdot \frac{\mathrm{d}t}{\mathrm{d}t} \right\} \qquad \text{eq. (A.15)}$$

And then elaborated by plugging eq. (A.14):

$$\frac{\mathrm{d}^2w}{\mathrm{d}t^2} = \frac{\mathrm{d}}{\mathrm{d}t} \left\{ \frac{\mathrm{d}w}{\mathrm{d}\alpha} \cdot (-v) + \frac{\mathrm{d}w}{\mathrm{d}t} \cdot (1.0) \right\} \qquad \text{eq. (A.16)}$$

Finally, it becomes:

$$\frac{\mathrm{d}^2w}{\mathrm{d}t^2} = \frac{\mathrm{d}^2w}{\mathrm{d}t \cdot \mathrm{d}\alpha} \cdot (-v) + \frac{\mathrm{d}^2w}{\mathrm{d}t^2} \qquad \text{eq. (A.17)}$$

The 1st term can be defined as follows:

$$\frac{\mathrm{d}^2w}{\mathrm{d}t \cdot \mathrm{d}\alpha} \cdot (-v) = \frac{\mathrm{d}}{\mathrm{d}\alpha}\left(\frac{\mathrm{d}w}{\mathrm{d}t}\right) \cdot (-v) \qquad \text{eq. (A.18)}$$

By substituting eq. (A.13), it becomes:

$$\frac{\mathrm{d}^2w}{\mathrm{d}t \cdot \mathrm{d}\alpha} \cdot (-v) = \frac{\mathrm{d}}{\mathrm{d}\alpha}\left(\frac{\mathrm{d}w}{\mathrm{d}\alpha} \cdot \frac{\mathrm{d}\alpha}{\mathrm{d}t} + \frac{\mathrm{d}w}{\mathrm{d}t} \cdot \frac{\mathrm{d}t}{\mathrm{d}t}\right) \cdot (-v) \qquad \text{eq. (A.19)}$$

Elaborating, similar to eq. (A.14), it becomes:

$$\frac{\mathrm{d}^2 w}{\mathrm{d}t \cdot d\alpha} \cdot (-v) = \frac{\mathrm{d}}{\mathrm{d}\alpha} \{ \frac{\mathrm{d}w}{\mathrm{d}\alpha} \cdot (-v) + \frac{\mathrm{d}w}{\mathrm{d}t} \cdot (1.0) \} \cdot (-v) \qquad \text{eq. (A.20)}$$

Finally, the 1st term is evaluated as follows:

$$\frac{\mathrm{d}^2 w}{\mathrm{d}t \cdot d\alpha} \cdot (-v) = \frac{\mathrm{d}^2 w}{\mathrm{d}\alpha^2} \cdot (v^2) - \frac{\mathrm{d}^2 w}{\mathrm{d}t \cdot d\alpha} \cdot (v) \qquad \text{eq. (A.21)}$$

Afterwards, the 2nd term is found straightaway as in eq. (A.17). Combining both terms from eq. (A.17) and eq. (A.21), then the second time derivative is formalized:

$$\frac{\mathrm{d}^2 w}{\mathrm{d}t^2} = \frac{\mathrm{d}^2 w}{\mathrm{d}\alpha^2} \cdot (v^2) - \frac{\mathrm{d}^2 w}{\mathrm{d}t \cdot d\alpha} \cdot (2v) + \frac{\mathrm{d}^2 w}{\mathrm{d}t^2} \qquad \text{eq. (A.22)}$$

And when $\alpha = 0$, both terms $\frac{\mathrm{d}^2 w}{\mathrm{d}\alpha^2} \cdot (v^2)$ and $\frac{\mathrm{d}^2 w}{\mathrm{d}t \cdot d\alpha} \cdot (2v)$ vanish due to continuity (Wolfert, 1999).

Then, ultimately, the extra terms in the equation of motion cancel again.

❖ Kinematic invariant

Later on in section 4.1.2, the assumed (steady-state) solution is an exponent with the following form:

$$w(x,t) = \sum X e^{i(\omega t - \gamma x)} \qquad \text{eq. (A.23)}$$

where X represent the amplitudes of the harmonic waves, ω the frequency and γ the wavenumber. Another wave characteristic to be defined here is the phase which is formulated from the argument of the exponent as seen here:

$$\phi = (\omega t - \gamma x) \qquad \text{eq. (A.24)}$$

And if the waves to be harmonic, this phase has to remain unchanged, which means:

$$(\frac{\mathrm{d}\phi}{\mathrm{d}t} = \omega - \gamma \frac{\mathrm{d}x}{\mathrm{d}t}) = 0 \qquad \text{eq. (A.25)}$$

Considering the time derivative of space being the velocity $\frac{\mathrm{d}x}{\mathrm{d}t} = v$ and substituting that in eq. (A.25), then we obtain the kinematic invariant:

$$\omega = \gamma v \qquad \text{eq. (A.26)}$$

❖ Rail irregularity due to temperature increase

In this section, the effect of axial stresses is included in an indirect way. Namely, by imposing an irregularity to the rail which can come from the deformation experienced by the rail due to increased axial forces

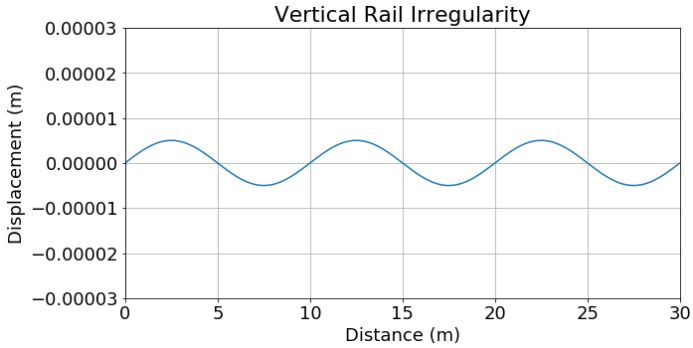

Figure A.2 Assumed rail deformation in the presence of thermal expansion

The picture here displays a rail irregularity function representing the expected rail behavior which can undergo some deformations under thermal loads. This irregularity function (which is assumed based on just a scientific/engineering feeling) is imposed in the rails as an attempt to check the consequences of rail deformations in terms of the response.

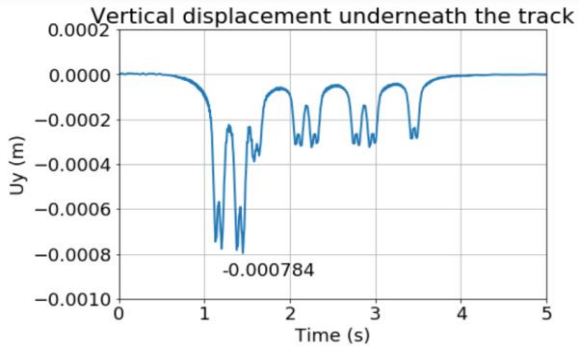

Figure A.3 Response vibrations (Neutral model)

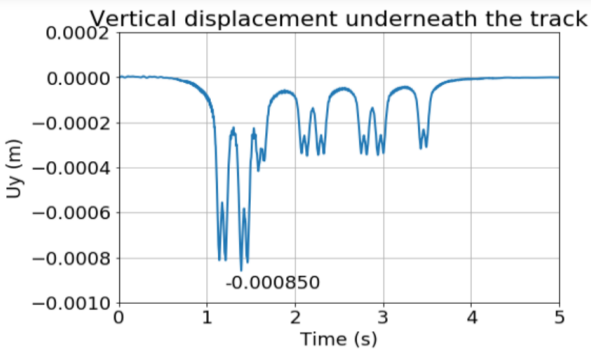

Figure A.4 Response vibrations (with rail deformation)

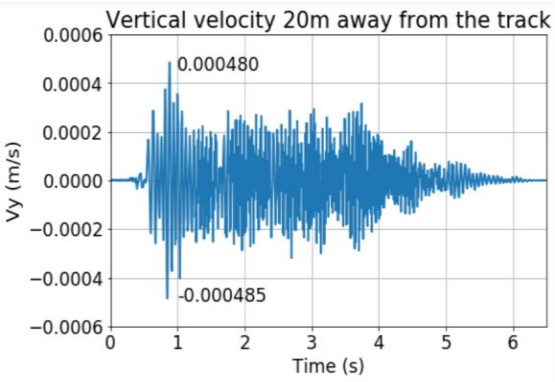

Figure A.5 Response vibrations (Neutral model)

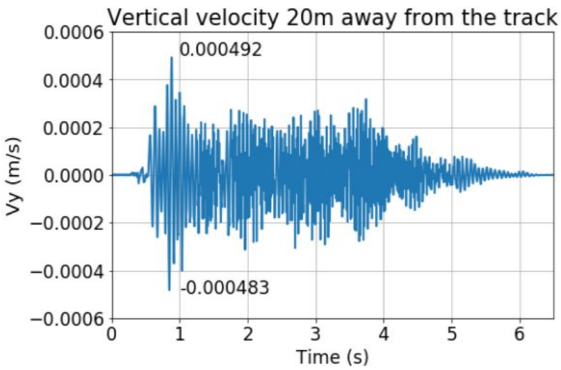

Figure A.6 Response vibrations (with rail deformation)

Not surprisingly, both the displacement plots measured under the track and the velocity plots 20 meters away from the track, show that the deformed rail model experience a higher response. The displacement fields announce an amplification of 9%, while the velocities do not exceed a 3% elevation. Taking a closer look at the graphs, no qualitative difference in the response is noted at all, while quantitatively a small difference is observed as stated earlier. In terms of the noise in both graphs no variation is noted between both graphs which indicate the similarity between both models. But ultimately, when the rail irregularity gets a higher amplitude or frequency, the response increases the level of noise gets affected just as well.

Bibliography

A.K. Ashmawy, R. S. (1995). Soil Damping and Its Use in Dynamic Analyses. *International Conferences on Recent Advances in Geotechnical Earthquake Engineering and Soil Dynamics. 9.* (pp. 1.13-1.21). St. Louis: Scholars' Mine.

A.V. Metrikine, H. D. (1999). Lateral vibrations of an axially compressed beam on an elastic half-space due to a moving lateral load. *European Journal of Mechanics - A/Solids*.

Aires Colaço, P. A. (2015). The influence of train properties on railway ground vibrations. *Structure and Infrastructure Engineering*, 517-534.

Amir M. Kaynia, C. M. (2000). Ground Vibration from High-Speed Trains: Prediction and Countermeasure. *JOURNAL OF GEOTECHNICAL AND GEOENVIRONMENTAL ENGINEERING*, 531-537.

B. Ghahremannejad. (2003). *Thermo-mechanical Behaviour of Two Reconstituted Clays.* Sydney: Department of Civil Engineering, Faculty of Engineering, University of Sydney.

Bombardier_TRAXX. (n.d.). Retrieved from wikipedia: https://nl.wikipedia.org/wiki/Bombardier_TRAXX

C Zhou. (2015). Effects of temperature and suction on secant shear modulus of unsaturated soil. *Gel̀ otechnique Letters*, 123-128.

C. Bayındır, A. S. (2018). *A Theoretical Method for the Investigation of the Effects of Soil Improvement on Train Induced Ground-Borne Vibrations.* Izmir: https://www.researchgate.net.

C. Zhou and C. W. W. Ng. (2015, September). Effects of temperature and suction on the stiffness of unsaturated. *Effects of temperature and suction on the stiffness of unsaturated*. Hong Kong.

Faragau, A. B. (2017). *Transition radiation in an inhomogeneous and nonlinear one-dimensional system.* Delft.

heat_distortion. (2009). Retrieved from shutterstock: https://www.shutterstock.com/search/heat+distortion te sturen.

Intercity-Express. (n.d.). Retrieved from wikipedia: https://nl.wikipedia.org/wiki/Intercity-Express

Intercitymaterieel. (n.d.). Retrieved from Wikipedia: https://nl.wikipedia.org/wiki/Intercitymaterieel

Juanjuan Ren, S. D. (2017). Energy Method Solution for the Vertical Deformation of Longitudinally Coupled Prefabricated Slab Track. *Mathematical Problems in Engineering* .

Kouroussis. (2012). *Influence of some vehicle and track parameters on the environmental vibrations induced by railway traffic.* Mons: Vehicle System Dynamics.

Kouroussis, C. C. (2012). *Investigating the influence of soil properties on railway traffic vibration using a numerical model.* Mons: Vehicle System Dynamics.

Laloui and Di Donna. (2013). *Energy geostructures : Innovation in underground engineering.* Lausanne: John Wiley & Sons, Incorporated.

Laloui and François. (2008, November). A constitutive model for unsaturated soils under non-isothermal conditions. *International Journal for Numerical and Analytical Methods in Geomechanics*.

Md. Abu Sayeed, S. M. (2016). *Investigation into Impact of Train Speed for Behavior of Ballasted Railway Track Foundations.* Australia: https://www.sciencedirect.com/.

NetworkRail_news. (2019, July 22). Retrieved from networkrail: https://www.networkrail.co.uk/news/western-route-ready-to-take-on-the-hot-weather-as-the-mercury-is-predicted-to-rise/

ns-icng. (n.d.). Retrieved from fromatob.nl: https://fromatob.nl/en/ns-icng/)

Onwuka, B. (2018). Effects of Soil Temperature on Some Soil Properties and Plant Growth. *Advances in Plants & Agriculture Research*, Volume 8 Issue 1.

P. Alves Costa, R. C. (2012). Track–ground vibrations induced by railway traffic: In-situ measurements and validation of a 2.5D FEM-BEM model. *"Soil Dynamics and Earthquake Engineering"*, 111 - 128.

Paul de Vos, S. (2017). *Railway induced vibration, state of the art.* International Union of Railways.

R. A. Broadbent, D. T. (2009). *EVALUATION OF THE EFFECTS OF TEMPERATURE ON RAILPAD PROPERTIES, RAIL DECAY RATES AND NOISE RADIATION.* Southampton: 16th International Congress on Sound and Vibration (ICSV16).

Rail_stressing. (2019, November 1). Retrieved from wikipedia: https://en.wikipedia.org/wiki/Rail_stressing

Railway_Buckling. (2016, February 28). Retrieved from youtube: https://www.youtube.com/watch?v=jJeiYaSFCf0

Sprinter. (n.d.). Retrieved from wikipedia: source: https://nl.wikipedia.org/wiki/Sprinter_(treindienstsoort)

Sun, L. (2016). *Structural Behavior of Asphalt Pavements.* Cambridge, Oxford: Elsevier.

Thompson, D. (2010). *Railway Noise and Vibration.* Oxford: https://www.sciencedirect.com/.

typeicr. (n.d.). Retrieved from martijnhaman.nl: http://www.martijnhaman.nl/typeicr.htm

U. Schneider, U. D. (1981). EFFECT OF TEMPERATURE ON STEEL AND CONCRETE FOR PCRV's. *Nuclear Engineering and Design*, 245-258.

Verruijt, A. (2017). *An Introduction to Soil Mechanics.* Delft: http://www.springer.com.

W. Gardien, A. S. (2003). *GEOVIB.* Utrecht: Movares (formerly Holland Railconsult).

Western route ready to take on the hot weather as the mercury is predicted to rise. (2019, July 22). Retrieved from Network Rail: https://www.networkrail.co.uk/

Wolfert, A. (1999). *Wave effects in one-dimensional elastic systems interacting with moving objects.* Delft.

z11307. (n.d.). Retrieved from treinposities.nl: https://treinposities.nl/foto/11307